DRONE BASED OUTDOOR INSULATOR INSPECTION

by

Danial Waleed

A Thesis Presented to the Faculty of the
American University of Sharjah
College of Engineering
in Partial Fulfillment
of the Requirements
for the Degree of

Master of Science in
Mechatronics Engineering

Sharjah, United Arab Emirates

April 2019

Approval Signatures

We, the undersigned, approve the Master's Thesis of Danial Waleed.

Thesis Title: Drone Based Outdoor Insulator Inspection

Signature	**Date of Signature** (dd/mm/yyyy)
_____ Dr. Shayok Mukhopadhyay Assistant Professor, Department of Electrical Engineering Thesis Advisor	_____
_____ Dr. Usman Tariq Assistant Professor, Department of Electrical Engineering Thesis Co-Advisor	_____
_____ Dr. Lotfi Romdhane Professor, Department of Mechanical Engineering Thesis Committee Member	_____
_____ Dr. Hassan Mir Professor, Department of Electrical Engineering Thesis Committee Member	_____
_____ Dr. Mohammad Jaradat Director, Mechatronics Engineering Graduate Program	_____
_____ Dr. Lotfi Romdhane Associate Dean for Graduate Affairs and Research College of Engineering	_____
_____ Dr. Naif Darwish Acting Dean, College of Engineering	_____
_____ Dr. Mohamed El-Tarhuni Vice Provost for Graduate Studies	_____

Acknowledgement

I would like to thank my advisors Dr. Shayok Mukhopadhyay, Dr. Usman Tariq and Dr Ayman-El-Hag for providing knowledge, guidance, support, and motivation throughout my research stages. I am deeply beholden for their great assistance, worthy discussion and suggestions.

I would also like to thank the professors of the Mechatronics Engineering graduate program who taught me master level courses that helped shape my skills. I really appreciate their advice and motivation.

I would also like to thank my fellow peers. Omar Ali, Mirghani Moutaman, Mohammed Ameen Tily, Ali Qahtan, Koshish Koirala, Fares Al-khawaja, Mohammad Shihab Awal and Hafiz Usman Butt who all have had a significant impact on my development as a master's student. Special mention to Hassan Umari whose helping nature and constructive advice has always been helpful and he has been one of the best mentor/friend that I have had in my academic carrier. I would also like to thank Wasim Al-Masri who has also been very influential in my teaching assistant role as he always had confidence in my teaching methods. Lastly, I would like to thank Mohammed Hussein who has been my group member in all the projects that I have done in my master's and his presence has always been welcomed in my work. Hussein's advice has always been critical but in a very constructive manner and the best thing that I have learned from him is to find ways of doing work efficiently rather then doing it tediously.

And finally, I would like to thank the American University of Sharjah for the opportunity to be a Graduate Teaching Assistant.

Dedication

This work is dedicated to my family and friends...

Abstract

Over the past few decades, interest in unmanned aerial vehicles (UAVs) and in particular quadcopters has increased due to the wide range of possible research applications that can benefit from the use of quadcopters. Insulator inspection on overhead power lines has traditionally relied heavily on visual inspection. The task is both cumbersome and relies on the experience of the inspector. It is also extremely dangerous as the inspector needs to work in close proximity with overhead power lines, and contact with these lines can lead to instant death. This thesis focuses on the development of a quadcopter based system that is able to inspect insulators on overhead power lines. The proposed system consists of a quadcopter that is able to inspect the health of insulators on an overhead power line. The quadcopter, via the help of its onboard cameras and Raspberry Pi based computer, is able to detect the health of an overhead power line insulator and simultaneously send images to the ground station where they are processed. The main contribution of this thesis is the development of a complete quadcopter based system for overhead power line insulator inspection. The offshore image processing algorithm presented in this thesis has a mean average precision of 0.66 and an average processing time of 0.55 seconds. The onboard image processing algorithm has a mean average precision of 0.26 and an average processing time of 1.28 seconds. These numbers show that quadcopter based insulator inspection can be carried out successfully using both offshore and onboard image processing techniques both in terms of precision and image processing time.

Keywords: ***Insulator Inspection; Quadcopter; UAV; Drones; RCNN; Image processing; tensorflow***

Table of Contents

List of Figures

List of Tables

List of Abbreviations

ACF Aggregate Channel Features

APT Average Processing Time

BLDC Brushless DC Motor

CIGRE Council on Large Electric Systems

DCC Distribution Control Center

DGPS Differential Global Positioning System

ELEVA Electric Power Line Exploration Using Aerial Vehicle

EPDM Ethylene Propylene Diene Monomer

EPR Ethylene Propylene Rubber

EPRI Electric Power Research Institute

ESC Electronic Speed Controller

FRP Fiber Reinforced Plastic

GFR Glass Fiber Reinforced

GPS Global Positioning System

HOG Histogram of Oriented Gradients

IMU Inertial Measurement Unit

IoU Intersection of Union

IR Infrared

mAP Mean Average Precision

PTFE polytetrafluoroethylene

RC Remote Controller

RCNN Region Convolution Neural Network

RGB Red, Green and Blue

ROS Robot Operating System

RTU Remote Terminal Unit

SR Silicone Rubber

STRI Swedish Transmission Research Institute

SVM Support Vector Machine

UAV Uanmanned Aerial Vehcile

UV Ultraviolet

Chapter 1: Introduction

This chapter provides a brief overview of the research work being carried out using quadcopters at present and its potential in carrying out cumbersome tasks easily. Further sections of this chapter deal with the thesis objective and research contributions that have been made by completing this thesis.

1.1. Overview

The field of unmanned aerial vehicles (UAVs) has seen rapid development in the past few years. Quadcopters are a particular type of UAV with four rotors and have attracted research interest [1, 2]. As the commercialization of quadcopters has increased, so has the research into different possible applications of quadcopters. One area of research related to quadcopters is in search and rescue missions such as locating people in rubble from buildings destroyed due to earthquakes, or helping locate people in buildings that have caught fire. In [3–6] further applications are mentioned such as their use in wildfire suppression, disaster and emergency management and border patrol. Other commercial applications include aerial photography, which not only has recreational uses but also can be used to study volcanic activities and atmospheric changes.

Another field of research that has seen a rapid increase of interest is the field of quadcopter based inspection of overhead power lines. Traditionally, overhead power lines have mainly inspected visually, where an inspector physically observes the overhead power line in order to determine if the cable or insulators and line accessories have defects or not. This approach is cumbersome, time-consuming and dangerous. Furthermore, the approach relies heavily on the experience of the inspector. In order to better enhance this procedure and provide safety to the inspector, quadcopters can be used to inspect the overhead power lines as the one discussed in [7]. Because numerous parts of overhead power lines need inspection and each component requires unique techniques, thus the field of quadcopter based inspection of overhead power lines has the potential for significant amount of research.

1.2. Thesis Objectives and Contribution

The aim of this work is to propose an image processing based technique that allows for the identification of the current health of ceramic insulators. The proposed algorithms will classify the insulators in three categories namely '*Healthy Insulators*', '*Dirty Insulators*' and '*Broken Insulators*'. Each category indicates the current health of the insulator where '*Heatlthy*' signifies that the insulator is in a good condition. '*Dirty*' signifies that the insulator has been polluted and '*Broken*' signifies that the insulator is physically damaged. The details of the image processing algorithms are discussed later but the main focus is on using algorithms that are reasonably accurate and precise while also not computational heavy so that they can be implemented on a small computer such as Raspberry Pi. Consequently the proposed algorithms will be able to work on a quadcopter (onboard) and also on a remote PC (off shore). As a result the proposed methodology can allow for both remote inspection and in-flight inspection using quadcopters.

The novelty of the proposed work is a complete quadcopter based overhead power line insulator health monitoring system. The image processing algorithms used are not only capable to be used on offshore computers, but can also run onboard on a small computer installed on a quadcopter.

1.3. Thesis Organization

The rest of this thesis is organized as follows. Chapter 2 provides a review of existing quadcopter and UAV based techniques that are currently being used for overhead power line inspection. In addition to this the literature review also focuses on types of insulators used in the industry and the method used to inspect them. Based on the literature review the processes of formulating an overall quadcopter system that can inspect the health of overhead power line insulators is discussed in Chapter 3. Furthermore, chapter 3 focuses on image processing techniques and basics of quadcopter systems. Chapter 4 discusses the results obtained by the system developed in Chapter 3. Chapter 5 provides concluding remarks on the work done in this thesis.

Chapter 2: Literature review

2.1. Inspection Techniques For Overhead Power Lines Via Image Processing

A thorough study in [8], provides useful insight about the available technology being used for detecting defects in overhead power lines. Most research caters to detection of defects in cables and towers that form the bulk parts of overhead power lines. Currently the techniques on overhead power line inspection using image processing can be divided into two categories. 1) UAV based techniques and 2) Non UAV based techniques. Because image processing is computationally heavy, therefore UAV based inspection tasks in both above categories do generally employ some post processing of images captured during flight.

2.1.1. UAV based techniques. In [8] it is mentioned that most of the research that has been carried out on UAV's is focused towards image-based recognition. The application mainly focuses on either mapping overhead power line in a given area or on inspecting various components of overhead power line. One image based detection technique discussed in [8] uses neural filter along with Hough transform in order to locate objects of interest in an image. This was done in order to locate overhead power lines in an image in order to inspect them. It was also suggested to use line clustering in order to refine the detection results. Another approach mentioned is to use an adaptive threshold to isolate power lines in varying light conditions. In addition to this, another approach is to form detailed 3D models of power lines via images acquired from a UAV in order to form 3D geometrical maps of overhead power lines. Furthermore, another study presented by [8] focused on automating the procedure of detection and tracking of overhead power line towers. The procedure used neural network based classification to detect towers and a helical tracking method.

In [9, 10] further work is done on overhead power line inspection using automated gimbals and manually operated helicopters. The concept is to first of all form a tracking algorithm that can detect poles on power lines using image processing. Once the location of a pole has been established in an image, then the camera attached to the gimbal can keep tracking the pole. In order to initiate the processes, the position of

a known power pole is provided using differential global positioning system (DGPS). Once tracking has been initiated a user then uses the images captured from the camera to inspect equipment on the overhead power line pole and to inspect object of interest close to the vicinity of the pole. It is important to note that the research done in [10], primarily focuses on overhead power line pole tracking. This is done by obtaining a steady stream of data from an automated gimbal mounted on a helicopter that is manually controlled. Thus no image processing is done in order to detect objects on the overhead power line poles and on power lines themselves which means an operator still needs to go through the images collected by the helicopter and locate the problems manually.

Detection of damaged cables on overhead power lines using image processing techniques is further studied in [11]. As in [10], the process requires helicopters to record a video of overhead power lines. Once the recording has been done, the video is then processed in order to check for two particular cable related problems. The first problem tackled is to observe the contour of the cable in order to find out if it has been physically cut from a particular point or not. The second problem tackled by the image processing algorithm is detection for the presence of arc marks using brightness of each frame recorded. One key issue is that the processes is not designed for real time monitoring.

A group from University of Wales has worked on the formation of a ducted fan rotorcraft for overhead power line inspection. According to [12] a ducted rotorcraft design was used as it is believed to be much safer due to the fact that rotors are enclosed by ducts and as a result it does not harm the surroundings if contact occurs between the rotors and surroundings. Further modification to the design presented in [12] is mentioned in [9]. According to [9] by adding position and attitude control [13, 14] along with a guidance system [15] and a power pick-up (shown in Figure 2.1) a more comprehensive device can be formed that can be autonomous and cover longer distances along overhead lines. Unfortunately details on what particular problem the device can tackle, and the image processing techniques used are not discussed in [12]. In addition to the previous work, another project entitled the "Electric power Line Exploration using Aerial Vehicle" (ELEVA) has also been mentioned in [9]. The main objective

of this project is to design an autonomous helicopter that can fly along power lines using stereo computer vision. Furthermore, the image processing algorithms does not only allow for tracking of the cable but it also enables conductor inspection as well. Figure 2.1 shows the prototype design for the UAV's discussed in [9].

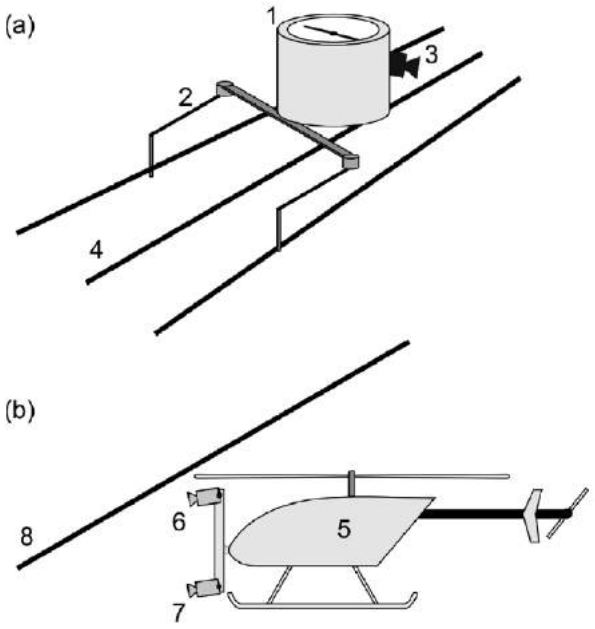

Figure 2.1: (a) Flying robot in development by the University of Wales research group; 1 rotorcraft; 2 power pick up mechanism; 3 camera used for power line tracking and obstacle avoidance; 4 power lines. (b) The ELEVA project flying robot; 5 helicopter; 6 and 7 the cameras used for stereo vision; 8 power line [9].

In [7], a novel method for joint inspection is provided that uses infrared cameras installed on a quadcopter in order to carry out unmanned inspection. The design of the UAV constitutes an infrared (IR) camera and red,green and blue (RGB) camera along with a video transmitter. The quadcopter uses mission planning software running on the ground control station to maneuver from one way point to another. The video transmitter sends images from IR and RGB camera to the ground control station where the images are processed. The algorithm processes the images in three steps. The first is by removing the background of the image in order to better locate joints in the image. The next step is to locate the joints. This is done by locating the hottest region in the foreground image. In theory the hottest region represents the joints in an overhead

power line tower and thus temperature thresholding is being used to locate the joints. Once the joints have been located further temperature thresholds are implemented to observe if the joints located have problems or not. Since the processing is done on the ground station further details are required in order to understand if the processing is done in real time or not. One of the major drawbacks of such implementation is that if the ground station is close to the vicinity of the area being investigated then real time processing can be carried out. However, due to the nature of overhead power lines the investigated area usually is not small. Thus information provided in [7], is not clear as to what happens in cases where the communication between the quadcopter and ground station breaks or cannot be established. In [8], one of the approaches for a fully autonomous system named RELIFO is provided. This approach uses visual data obtained from cameras attached to the UAV in order to detect the distance between the conductors and the objects close to it such as buildings and vegetation. The UAV is equipped with thermal and visual cameras. The visual cameras are used to provide line tracking for the UAV so that it can follow the overhead power line. The cameras are also used for stereoscopic analysis in order to detect objects close to the overhead power line. The thermal cameras are used for damage detection on the conductors. From the works mentioned above it can be noted that UAV based inspection is still in its infancy with regards to overhead power line inspection.

2.1.2. Non UAV based techniques. The methods provided in the previous section relied on image based detection techniques. However, in most above cases the images are processed after the inspection has been carried out via a UAV. This section focuses on the work done so far in the field of image based detection techniques that do not require UAVs in order to inspect overhead power lines. Most aerial inspections are still carried out using helicopters and inspection personnel use cameras and visual cues in order to carry out the inspection. In [16], a method of remote monitoring for overhead power line towers is proposed. It is argued that in developing countries where infrastructure is not that well developed and areas where inspection via aerial vehicles is difficult due to harsh terrain and weathers, a remote monitoring system would be more beneficial. The main idea in [16] is to install cameras on overhead power line

towers that can take images of the insulators installed on the tower periodically. Further hardware includes remote terminal units (RTUs) that send the data from the tower to the distribution control center (DCC) where the actual image is processed.

The image processing is divided into 6 steps. Step 1 is to read the image and send it to the DCC. In step 2, the DCC converts the RGB image to L×a×b color space. In Step 3, the k-means clustering algorithm is applied and the desired clusters are acquired. The desired cluster include the pole, cross-arms, insulators and conductors. In step 4, the pixel intensity values close to the clusters found in step 3 is set to zero. In step 5, the pixel intensity is computed row-wise, column-wise and diagonally. If the intensity count is greater than a specified threshold a bounding box is drawn around the surrounding pixels. In the last step the region from the bounding box is passed through a pre-trained adaptive neuro-fuzzy inference system that determines whether the bounding box contains an insulator and also its state of health. The work presented in [16] distinguish the state of insulators in two categories. The first is that the insulator is healthy and the second is that the insulator is broken. Similarly work done in [17] uses images taken from the overhead power line towers via cameras and RTU. The main approach is to again first segment insulators in a image and then use wavelet and support vector machines (SVMs) in order to determine the state of the insulators. Details of the algorithm and its detection criteria can be found in [17].

In [18], edge detection is used based on images captured from a cameras attached to overhead power line towers. It is proposed that by using edge detection with Canny edge detector can help locate cables on overhead power line towers easily. The paper introduces a custom Canny edge detector that can help in detection of wires on overhead power line towers easily. According to the authors the results obtained by using just edge detection with Canny operators can result in false detection. However, by improving the threshold using an automatic identification threshold, improvements can be made on the existing Canny operator. Result from [18] show that improvements were indeed observed for wire detentions on overhead power lines.

From the literature review above it can be clearly seen that a considerable amount of work has been done on overhead power line inspection. However, not a lot of work exist on insulator inspection using UAVs or quadcopters. The core of this thesis is on

insulator inspection via quadcopters. Therefore, the next section provides a through review of insulators used in overhead power lines.

2.2. Insulators

Insulators used in overhead power lines are categorizes by two main properties. These properties are the material from which the insulator is made and the second is the application for which the insulator is used for. Two different materials have been used in outdoor insulators, namely, ceramic and polymeric materials. This section provides a brief introduction for each type and provides some advantages and disadvantages of each type discussed.

2.2.1. Ceramic. According to [19], ceramic insulators (made of porcelain and glass) were first used around 1880. Porcelain has been used as an insulator in overhead power lines for more than a century. It has been used for such a long time because of its stability due to the strong ionic bonding present in it. The source of this bonding comes from the bonds formed between silicon and oxygen. The ionic bonding present in porcelain yields a highly stable material that highly decreases reactivity towards UV, humidity and other similar environmental factors. Furthermore, porcelain based insulators provide mechanical support to the cable. Another reason for its popularity is it's low-cost of production [19]. Porcelain, however, does suffer from few drawbacks as well, for example, ceramic insulators made from porcelain are brittle in nature and thus susceptible to mechanical damage [19]. Another major disadvantage of the ceramic insulator is its weight. Since ceramic insulators are quite heavy it is difficult to use them in overhead power lines with extra high voltage. This is one of the primary reasons other lighter weight insulators were introduced. Furthermore, ceramic insulators tend to perform poorly when their surface is contaminated. In particular, the hydrophobicity of the insulator is greatly decreased, which increases the chances of flashover. A flashover occurs when the air around or along the insulator breakdowns and conducts electricity. Figure 2.2 shows a typical ceramic insulator used in the industry and Figure 2.3 shows parts of a ceramic insulator.

Figure 2.2: Ceramic insulator.

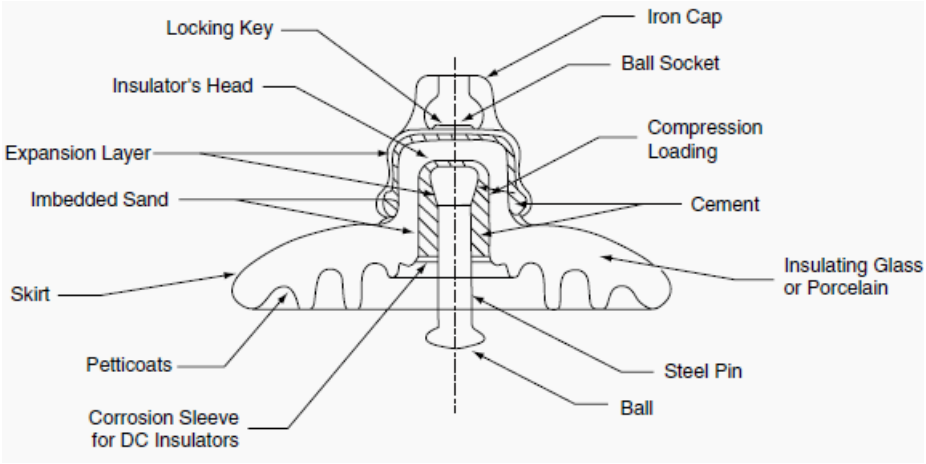

Figure 2.3: Parts of a ceramic/porcelain insulator [20].

2.2.2. Polymer. Polymer insulators were first introduced somewhere between 1930s and 1940s. However, at that time their performance was not as good as expected, and their use was put on hold [21]. By the 1970s development in the field had led to the formation of materials such as ethylene propylene rubber (EPR), ethylene propylene diene monomer (EPDM), polytetrafluoroethylene (PTFE), silicone rubber (SR), and a core of fiber-reinforced plastic (FRP), all of which can be used in the formation of overhead power line insulators. With the presence of these materials, the industry started to shift from ceramic to polymer insulators.

The shift in the industry could have been motivated by the advantages polymer insulators provided. One of the main advantages of polymer insulators is their superior pollution performance due to its hydrophobic surface. The cost of production and its installation is also comparatively cheaper than that of ceramic insulators. On the other hand, polymer insulators are prone to weather degradation and thus are highly susceptible to environmental conditions such as UV, moisture, humidity that cause damage to the polymer surface as discussed in [21]. Figure 2.4 shows a polymer insulator used in the industry and Figure 2.5 shows parts of a polymer insulator.

Figure 2.4: Polymer insulator [22].

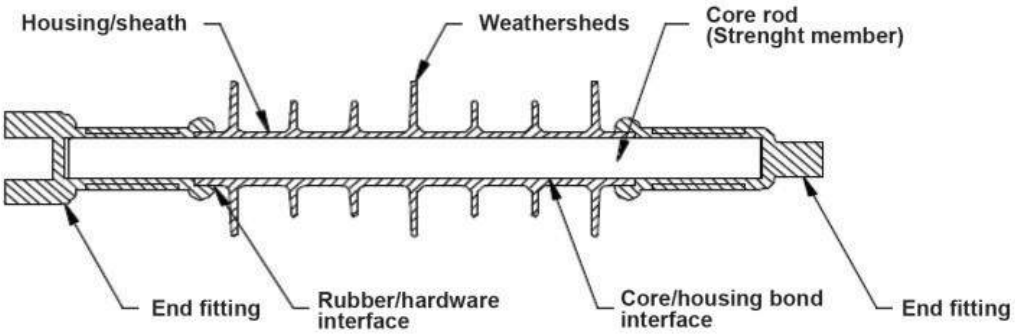

Figure 2.5: Parts of a polymer insulator [23].

2.2.3. Insulators types based on application. The industrial application of insulators can be divided into three main categorizes. In these categories the insulator can be either made up of ceramic or polymer. Figure 2.6 shows all three types of insulators and brief description on each category is provided below.

Pin insulators were the earliest insulators to be implemented on overhead power lines. They are still used in the industry and have three variants that can withstand different level of high voltage. The maximum kV rating a three part pin insulator can handle is 33kV [24]. Post insulators are used for bus bars and switches which are used in substations for disconnecting. A post insulator is similar to a pin insulator but has a metal base. The post insulator has three variants line post insulator, switch post insulator and cut out switch insulator [24]. Suspension insulators are used in overhead power lines that have a rating above 33 kV, where it is not economically viable to use pin insulators. Suspension insulators consist of a disc shaped piece of porcelain and the surface underneath is grooved to increase the surface for the leakage path [24].

Figure 2.6: Insulator types: (a) pin insulator (b) post insulator and (c) suspension insulator [24].

2.2.4. Causes for defects. In [25], electrical stress on an insulator is linked to the break-down of an insulator. Factors that can generate electrical stress are linked to flashover and puncture. A puncture occurs in an insulator when the electrical discharge between the conductor and the insulator pin occurs through the body of the insulator. When a puncture occur the insulator is considered to be permanently damaged. The safety factor of an insulator is the ratio of puncture strength to flashover voltage. A high value of safety factor is desirable as it means that a flashover takes place before

the insulator gets punctured. Similarly according to [26] an insulator used in overhead power lines is considered damaged if it fails mechanically, and a flashover occurs on its surface, or deteriorates to the extent that the safety factor is compromised. Damage to insulators can be caused by thermal and mechanical cycling, ablation from weathering and electro-thermal causes, flexure, and torsion, ionic motion, corrosion, and cement growth.

Change in the operating temperature of insulators in known as thermal cycling. Since insulators are exposed to the outside environment, they experience a change in temperature due to the cycle of day and night. This change in temperature causes cracks on the insulators as a result of thermal expansion and contraction on a daily basis. Leakage current on the insulator surface is also a thermal source and causes the insulator to warm up pretty quickly. The cement present in the insulator experiences expansion. This expansion is caused by wetting of the cement due to rain or high humidity and causes cracks on the insulator. Cement growth can also be caused by contaminants in the atmosphere such as sea-salt, road-salt and certain types of sulfates as they attack the Portland cement found in the insulators. According to [27], the insulators most prone to cement growth related damages are the ones present on the dead end strings(insulators attached to the pole) and insulators on the windward side (The side facing the wind) of a tower. Figure 2.7 shows an insulator that has been contaminated by a mixture of salt and dirt deposition.

Figure 2.7: Insulator suffering from salt and dirt contamination and discoloration [28].

Moreover, these contaminants can also cause corrosion inside the insulator if the contaminants penetrate through the surface of the insulator [26]. If such type of contamination is allowed to be built up on the insulator, it can greatly increase the probability of having a flashover on the insulator surface.

2.2.5. Types of defects. Mechanical failure of an insulator can be divided into three subcategories. These failures are categorized as 1) Normal break of glass fiber reinforced (GFR) rod, 2) Brittle fracture and 3) Slip at the end of the fittings [29]. Explanation of each category is given below.

2.2.5.1. ***Normal break of GFR.*** The GFR rod is the core rod as seen in Figure 2.5 is completely elastic until its damage limit. Unfortunately, no specific reasons as to what causes this damage are known, but from the type of damage, it can be assumed that this might be caused by the expansion and contraction of the GFR due to change in temperature.

2.2.5.2. ***Brittle fracture.*** Brittle fracture is considered to be caused by stress corrosion and is initiated by the simultaneous application of mechanical stress along with diluted acids [30]. In most cases it occurs close to the high voltage ends where the insulator faces high level of electrical and mechanical stresses. Figure 2.8 shows a brittle fractured insulator.

Figure 2.8: Brittle fracture on an insulator [30].

2.2.5.3. ***Slip at the end of fittings.*** This problem is no longer a common issue in insulators anymore. This problem occurs due to use of worn out tools being used to connect the ends of the GFR rods to the end fittings and also when the variation between the diameter of the GFR rod and the end fittings is not too large. As a result, cracks start to appear which may lead to the slip of the end fittings.

Unfortunately, insulators are often targets of vandalism. People sometimes use insulators as target practice; and thus insulators are hit by stones and gunshot. Figure 2.9 shows insulators that have been damaged due to vandalism. In the case of glass suspension insulators, the results are catastrophic as the outer shell of the insulator is completely damaged. In places where vandalism is high, polymer insulators are often used.

Figure 2.9: Damaged insulators due to vandalism [30].

In certain cases, bird droppings on insulators have been attributed to promoting flashovers in insulators. Since these bird droppings are considered to be conductive in nature they can help short out the air gap between the insulators. The potential; difference between these insulators is very high. This combined with the presence of the shorted air gap results in a flashover. It has been reported that flashover due to bird droppings contributed to 18.97% of composite insulator failure in China [31].

Bird pecking is another problem observed in the industry. In Australia, parrots have been observed to chew out most parts of the insulators thus exposing the GFR

rod [29]. In Switzerland, crows have been reported to peck on both the sheds and sheath of the insulator to such a degree that the rod inside the insulator becomes exposed to the environment [29]. Rodents have also been observed to chew on composite insulators, however, this is observed when the insulators are being stored on the ground in a warehouse [30]. Figure 2.10 shows an insulator that has been damaged due to bird pecking.

Figure 2.10: Insulator damaged due to birds pecking [30].

2.2.6. Insulator fault detection techniques. Detection techniques of insulators are traditionally done via visual inspection by trained personnel who use additional hardware in order to assist them in the inspection. However, as technology has progressed techniques have been developed that no longer require an inspector to be physically present thus these techniques can be divided into two groups which are 1) traditional visual hardware based techniques and 2) unnamed aerial vehicles based techniques. Techniques based on UAV have already been discussed in detail in the beginning of this particular chapter. It is however important to provide information on traditional techniques in order to get an idea of how cumbersome these techniques are and as result the need to improve upon them.

Visual inspection is currently the most reliable form for inspection of both overhead power lines and insulators. The inspectors are provided with detail description

of how to identify defects from guidelines provided by Council on Large Electric Systems (CIGRE), Electric Power Research Institute (EPRI) and Swedish Transmission Research Institute (STRI). These guides contain a detailed description of expected defects and are accompanied by color images of the defect for the ease of the user. The limitations of visual inspection are that it relies on the experience of the person carrying out the inspection. Moreover, visual inspection cannot detect defects that are inside the insulator.

Due to certain defects on the insulator surface, electrical discharges may start to take place in the form of partial discharge or leakage current. This causes the insulator to heat up hence infrared cameras are used to detect such defects as the damaged and now heated region are clearly visible on the IR cameras. The advantage of using infrared thermography is that it enables the user to detect defects that are inside the insulator and are not visible to the naked eye. A major disadvantage of infrared thermography is that it requires an insulator to be heavily damaged in order to detect a defect in it. This means that the technique cannot be used on insulators that are slightly damaged. Furthermore, the results further degrade if the humidity level is low [32, 33]. Figure 2.11 shows images taken by an infrared camera used for detecting internal faults in the insulator.

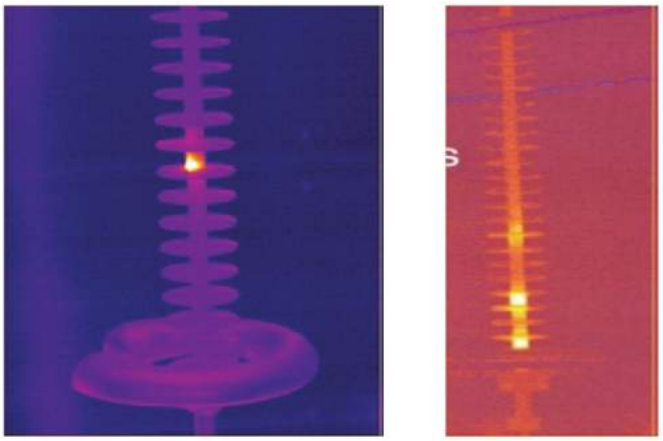

Figure 2.11: Insulator damage detection via infrared cameras [33].

As mentioned in the previous section, it is hard to detect damages to the insulator when most of the insulator is intact and the released energy from the defect is small.

Alternatively, corona cameras can be used to detect these defects. Corona cameras capture UV rays being emitted by the defect to detect the presence of corona and it is important to mention that different types of corona cameras are available that can detect corona in daylight as well as in the night. The cameras measure the intensity of the corona by calculating the number of pulses of light emission referred in the field as blobs. According to [33] corona detecting cameras still lack the ability to detect internal defects in an insulator but by exposing some inner part of the insulator some success can be achieved. Corona-based cameras can also work in dry conditions and thus tackle the issues faced by IR cameras. Figure 2.12 shows a camera capturing corona using UV.

Figure 2.12: “Blob” captured via daylight corona camera [33].

The existence of damage in outdoor insulators can alter the electric field distribution close to the vicinity of the insulator surface. A portable diagnostics probe can be used to measure the electric field near the insulator. The technique requires manual operation of a probe that needs to be kept close to the insulator being inspected. The mode of operation is to measure the electric field around an insulator and then compare the results with a reference fingerprint obtained from a healthy insulator [33]. Figure 2.13 shows results obtained from two different cases

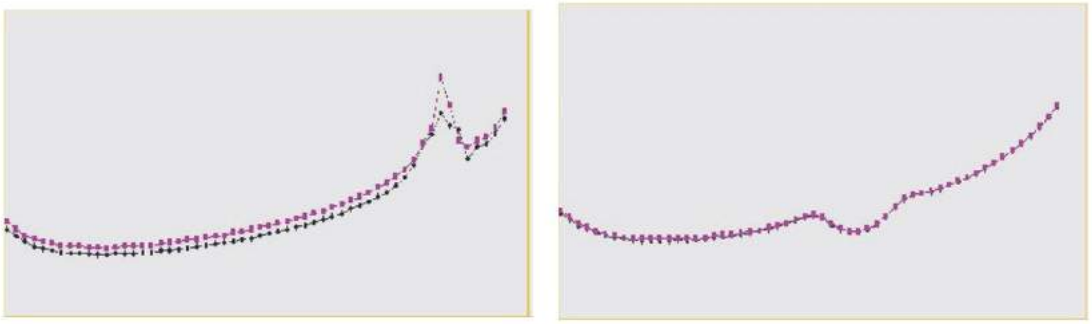

(a) (b)

Figure 2.13: Insulator defect detention using magnetic probe (a) at the fitting (b) in the middle [33].

Chapter 3: Methodology

Most of the real time monitoring of insulators found on overhead power lines is primarily done by installing cameras and remote terminal units (RTUs) on the overhead power line towers. The RTU then transmit the data to distribution control center (DCC) where the actual image processing takes place. Some of the disadvantages of such a systems is that it requires a lot of hardware to be installed on to the existing systems in order to become fully operable. In addition to this the cameras installed on a single tower can only work in the vicinity of the tower. This means that while the tower area is covered there is no coverage of the area in between the towers where defects and problem can arise. In addition to this regular maintenance of the inspection hardware also needs to be carried out along with inspection of the overhead power line towers which increases the overall maintenance cost of the overhead power line system. One of the main advantages of using a DCC is that it allows the user to carry out comprehensive checks on the images being transmitted from the RTU. As a consequence the image processing results are more precise and accurate and have high reliability.

An optimal solution would be to carry out real time monitoring on a system that can maneuver easily close to the vicinity of overhead power lines. Furthermore, the device should have capabilities of doing both onboard and offshore processing in real time. Doing so will form a system that can work independently and will not require a user to go through the data in post processing. In addition to this, image processing algorithms need to be properly selected so that they can provide results that are precise as well as provide fast output, a necessity if one has to successfully carry out inspection in real time.

The main focus of this thesis is on designing and testing an overall hardware and software based system that can carry out insulator inspection on an overhead power line. The main hardware consists of a quadcopter based system that can be controlled by an inspector while carrying out inspection. The software consists of image processing algorithms that will run on the quadcopter as well as on the ground station for simultaneous real time inspection. The basic architecture that the quadcopter system needs to follow is shown in Figure 3.1. This basic architecture will be used to design

and develop the required software and hardware components. Figure 3.2 shows how an operator needs to operate the quadcopter in order to carry out an effective inspection. Way points are the locations of the towers and the green arrows represent the quadcopter revolving around the tower in order to fully insulators on a tower from every angle possible.

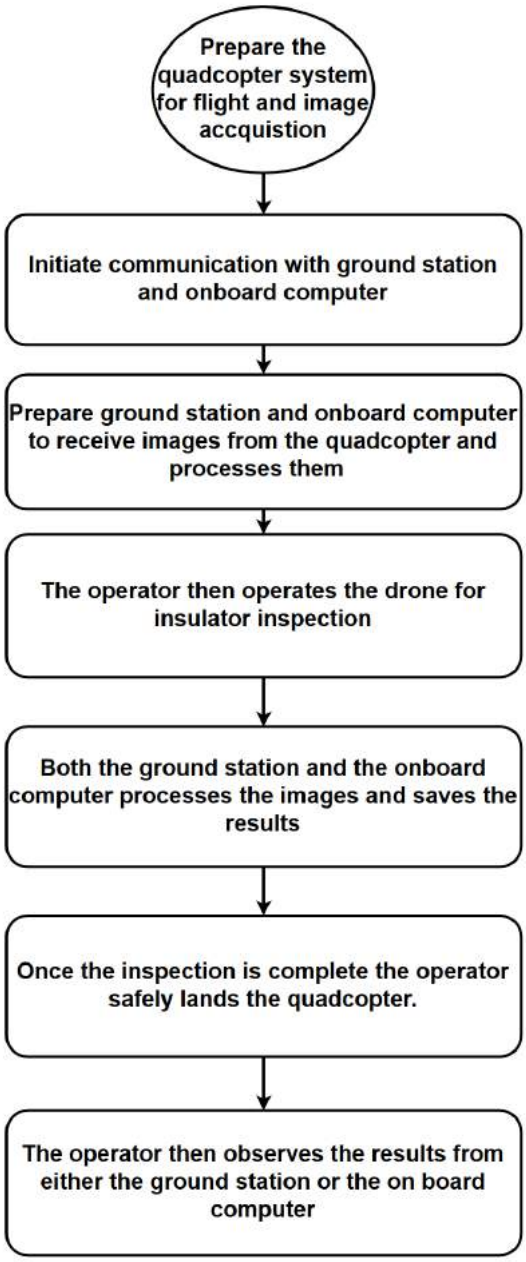

Figure 3.1: A flow chart showing the basic architecture of the targeted quadcopter system.

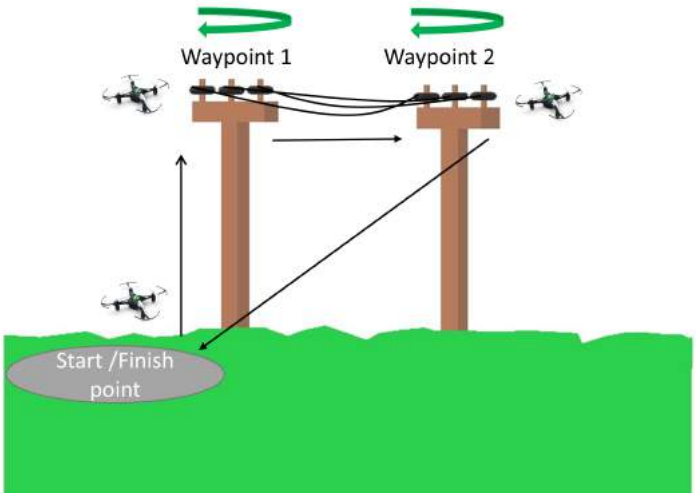

Figure 3.2: A representation of how the quadcopter will inspect the towers.

This section primarily analyzes the image processing algorithms considered for detecting insulators on an overhead power lines. For this particular study only ceramic insulators are considered but the work presented can be extended to other types of insulators, and the image processing algorithms can be modified if needed. This chapter also focuses on the overall hardware and software required to form a quadcopter systems that can detect three types of insulators on an overhead power lines. The types of insulators considered are '*Healthy Insulators*', '*Dirty Insulators*' and '*Broken Insulators*' Also the algorithms considered are such that detection of insulators is possible both onboard the quadcopter, and also possible on a ground control station computer.

3.1. Image Processing Algorithms For Offshore Processing

The first part of developing an image processing algorithm is to is to identify whether the algorithm needs to carry out image classification or object detection. In image classification the main objective is to identify whether a particular object of interest exist in a given image. In object detection algorithms the main objective is to identify whether an object exist in a given image and then locate the object of interest within the image as well. This is usually done by drawing a bounding box over the object of interest. This particular work focuses on object detection algorithms and is primarily trained to detect *Healthy Insulators, Dirty Insulators* and *Broken Insulators*.

3.1.1. Data for training. In order have an effective image processing algorithm that can detect objects in an image it is important to make a data set that contains known instances of the interested objects. In order to make such a data set, multiple images of the object of interest need to be taken, and then the objects of interest need to be labeled. The labeling of the object of interest helps in extracting major information about the object in a given image. Each label carriers the name of the object of interest. The bounding box contains the pixel information of the object in the image. While the formatting of the bounding box data may vary from application to application, in Matlab [34] bounding boxes contain [x y width height]. Where x and y represent the coordinates of the upper left corner of the bounding box in terms of pixels. The width and height represent the width and height of the box which is drawn around the object of interest.

A total of **2973** images were taken over in order to make the data set. In order to take a large amount of images and also vary the background and the lightning conditions several videos of the insulators were taken. The frames in each video were extracted and used as individual images in the training data set. Also, the videos were created so that the frames contained all scenarios that were thought to be faced by a quadcopter when carrying out an inspection. Most of the videos were taken by maneuvering around a custom built tower that can hold the insulators. Figure 3.3 shows the custom built insulator holding tower used for gathering image data.

Figure 3.3: Custom built tower for holding insulators.

3.1.2. Comparison of image processing algorithms. After completing the image data set, the next part was to look into image processing techniques that can be used for object detection. Several techniques were looked into [35–39], for locating objects in a given image.

In the initial stages point feature matching [36] was implemented on a smaller part of the data set. From the results it was observed that point feature matching is not a good way for detection of objects that have plain and repeating textures further more it is recommended that point matching system be used for objects that are unique and have a distinct features that can allow the algorithm to detect the object in a cluttered environment. This particular constrain is a major problem for the ceramic insulators that have identical shapes and structure, and thus point matching image processing technique was not used.

The next image processing algorithm that was considered for insulator detection is a cascade object detector using histogram of oriented gradients (HOG) [35] as the main feature that the algorithm uses for identifying the insulators in an image. Two major problems were faced when the trained cascade object detection algorithm was tested. The first problem was that the algorthim gave multiple results for a given object and also showed high confidence in false positive cases. The second problem was that identification of objects at varying distances was not precise at all. In cases when the object had a larger ratio than what was present in the training or the orientation of the object was different than the one the system was trained with, the results were not at all acceptable. One solution that was implemented was to increase the training data set of the training images but the problems still persisted with little to no improvements and so the cascade object detector was not further pursued.

After getting unsatisfactory results from the previous algorithms the focus then shifted on using aggregate channel features (ACF). Details on how ACF uses an image in order to train and detect can be found in [39]. The ACF detector can use a pretrained neural network model and modify it in order to detect new objects of interests. In our case when the systems was trained using a part of the whole data set, two major problems were found. The first is that in Matlab the training algorithm only supported a single label training, this meant that three separate detectors are required in order

to processes a single image, which essentially increases the overall processing time of the system. In addition to this when the algorithm is trained in order to detect broken insulators the results are not satisfactory as the detector detected small areas on the broken insulators rather than the whole insulator as a broken insulator. Figure 3.4 shows the results obtained by implementing the ACF object detector. Since the algorithm was not providing a substantial improvement in detection and required at least three different trained detectors for each object, it was decided not to further pursue it.

Figure 3.4: Results of AFC object detector for broken insulator inspection.

3.1.3. Regional convolution neural network (RCNN). After attempting the above algorithms focus then shifted on using regional convolution neural network in order to form an object detector that can detect all three type of insulators that we intended to investigate while carrying out an inspection. Steps provided in [40] were followed. In which, a pretrained network was used along with RCNN. This is known as transfer learning and was implemented in order to increase the overall all performance of the

trained system. The pretrained network that was used is called **CIFAR-10** [41] and is a network that was trained with 50000 images. Two advantages of using this network is that firstly, it decreases the overall time required to train the system. Secondly, a relatively small data set of around 100 images can be used to train the network for new object of interest. In addition to this, the algorithm is able to make improvements to the existing CIFAR-10 net in order to locate all three objects in an image with a single detector. This allows for multiple object detection in a single implementation, which is a major improvement to the work that had to be done in ACF based object detection. The convolution neural network consist of 15 layers which are shown in Table 3.1.

Table 3.1: Layers used to build the convolution neural network.

	Layer name	**Layer Description**
Layer 1	Image Input	32x32x3 images with 'zerocenter' normalization
Layer 2	Convolution	32 5x5 convolutions with stride [1 1] and padding [2 2 2 2]
Layer 3	ReLU	
Layer 4	Max Pooling	3x3 max pooling with stride [2 2] and padding [0 0 0 0]
Layer 5	Convolution	32 5x5 convolutions with stride [1 1] and padding [2 2 2 2]
Layer 6	ReLU	
Layer 7	Max Pooling	3x3 max pooling with stride [2 2] and padding [0 0 0 0]
Layer 8	Convolution	64 5x5 convolutions with stride [1 1] and padding [2 2 2 2]
Layer 9	ReLU	
Layer 10	Max Pooling	3x3 max pooling with stride [2 2] and padding [0 0 0 0]
Layer 11	Fully Connected	64 fully connected layer
Layer 12	ReLU	
Layer 13	Fully Connected	10 fully connected layer
Layer 14	Softmax	
Layer 15	Classification output	crossentropyex

Using the RCNN training processes these layers are added to our own modified CIFAR-10 based RCNN algorithm. From the compiled data set of 2973 images initially 990 images were used to form a prototype CIFAR-10 based RCNN algorithm.

Results obtained from the prototype algorithm showed major improvements then the previous discussed algorithms. The first improvement that was noticed was the modified CIFAR-10 network was able to detect all three types of insulators. The detection was able to identify all three categories with changing backgrounds. Secondly, unlike the previous algorithms, the detection made by the modified CIFAR-10 network usually had bounding boxes around the object of interest rather then detecting multiple parts of the same object. One of the main problems noticed was that the modified network still had problems in detecting insulators in certain perspectives and also had problems related to false negative detection as well. These problems were taken care by increasing the data set of the training from 900 to 2800 images, and using 173 images for verification. The settings for the training were not altered to the ones shown in [40]. After adding the extra images for training, improvements in the network were noticed and no further tweaking was done because, the modified CIFAR-10 based RCNN network was providing satisfactory results.

It is worth mentioning that further work was carried out in forming a Fast RCNN and Faster RCNN based on the intuition that it will improve the time required to processes the images. This however, was not the case. It was found that both RCNN and Faster RCNN were providing similar precision when it came to detection, but were in fact taking more time than RCNN to processes a given batch of images. Since our application is time sensitive, it was decided to not pursue the Fast and Faster RCNN.

3.1.4. Image processing algorithms on board. In the later stages of the thesis work it was found that the modified CIFAR-10 network cannot be directly implemented on the computer present on the quadcopter. This was mainly because the operating system running on the quadcopter is Ubuntu and the modified network was built on Matlab running windows. Another major problem is that the Ubuntu system present on the quadcopter is old and thus installing image processing algorithms on it will lead to problems on the operating system itself which jeopardizes the safe operation of the quadcopter. Therefore, it was decided to add a Raspberry Pi to the quadcopter for on board image processing. Fortunately, newer version of Raspbian support tensorflow which is an open source machine learning framework. By following the tutorial found in

[42], and by using the pretrained networks *ssd mobilenet v2 coco model* [43], an image processing network was formed that can run on the Raspberry Pi with sufficient speed. As with the offshore processing model, 2800 images were used for training and 173 images were used for verification. On testing the modified network on the Raspberry Pi, it was found that the algorithm can processes a single frame in approximately 2 to 3 seconds. While a lower time would have been better, no further work was carried out on reducing the time required for image processing as it was found that further improvements on the hardware cannot be achieved due to its limited processing power and lack of GPU support.

3.2. Quadcopter Basic Hardware and Software Components

According to [44,45] a basic definition of a quadcopter system can be defined as a helicopter which has four equally spaced rotors. These rotors are generally arranged at the corners of a square body and are typically pointing upwards. It is well known that quadcopters are underactuated as the overall body has six degrees of freedom, (three translation in x, y and z and three rotational degrees along x ,y and z which are primarily referred as roll, pitch and yaw) but only four motors. [44–47]. For the same reason controlling the quadcopter is challenging and as a result a lot of research has been carried out on improving the control methods for quadcopters. This thesis however does not delve into this problem. In the next subsections a brief summary of the basic components of a quadcopter is discussed in order to develop an understanding of the requirement and use of each component.

3.2.1. Overall setup. In order to form a quadcopter a combination of hardware and software is required. The hardware of the system can be divided into three sub categories. 1) Structural components and 2) Electrical components. In [6], an overall setup of a quadcopter systems is presented. The hardware of the system is divided into two categories. The blue box in Figure 3.5 represents the electrical and hardware components installed on the quadcopter air frame and the red region represents the hardware and software that encompasses the ground control system.

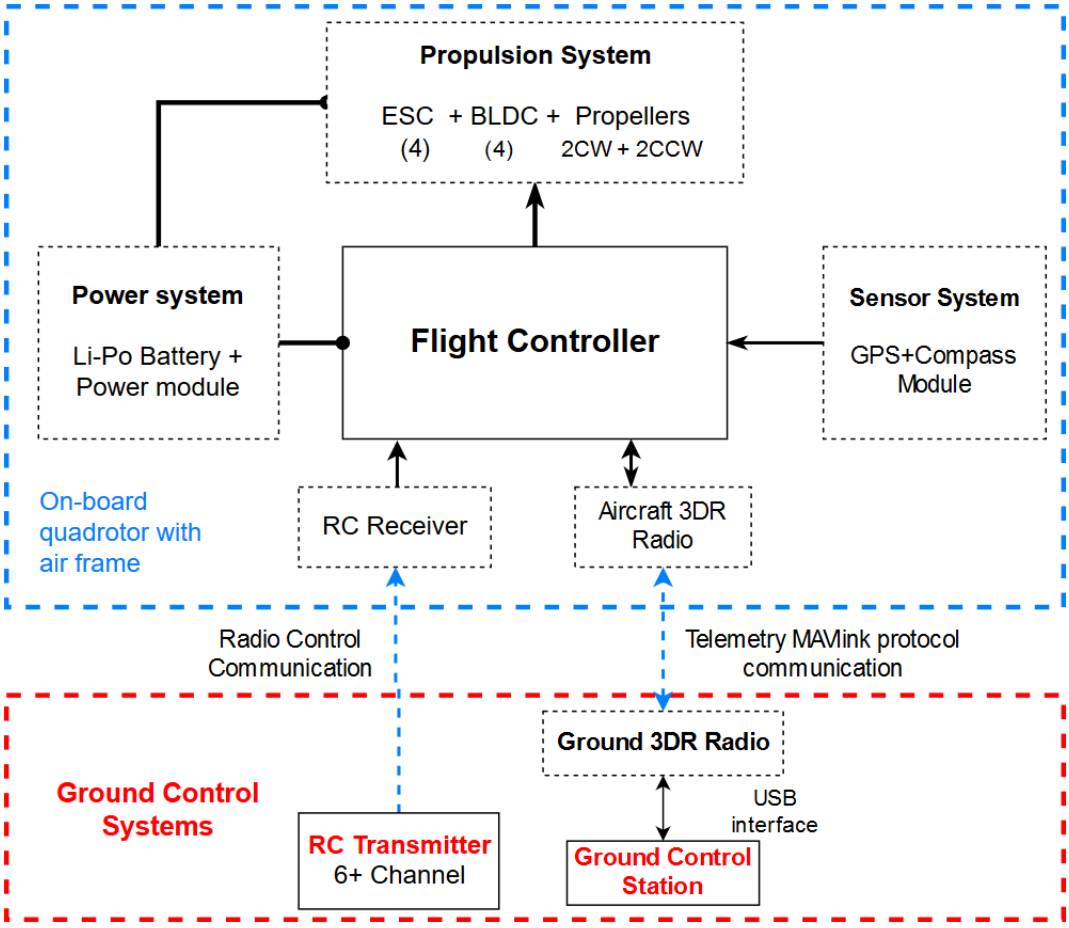

Figure 3.5: Overall setup of a quadcopter system [6].

3.2.2. Structural components. The structural components of a quadcopter consist of the frame, landing gear and propellers. Each of these components are essential to the quadcopter structure.

The material and size of the overall frame determines the quadcopter payload capabilities as well as its application. Traditionally small frames might be developed for prototyping, indoor applications, control algorithm testing and applications that do not require heavy payloads. Whereas large frames might be used for outdoor and heavy payload applications. Since quadcopters have four arms, the orientation of the frame is mainly divided into two categories. Figure 3.6 shows the two categories which are

popularly referred as the plus "+" and cross "x" orientation whereas Figure 3.7 shows an actual quadcopter frame.

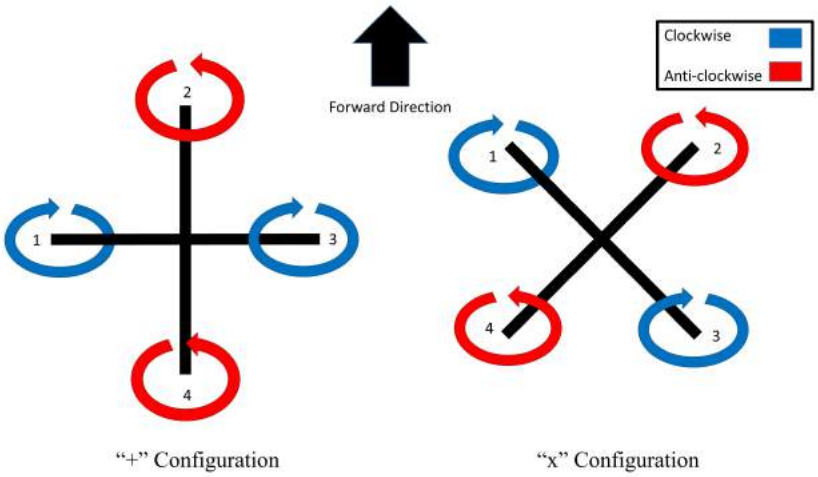

Figure 3.6: The two configurations popularly used for quadcopters and the rotations each propeller takes [45].

Figure 3.7: An example of a quadcopter frame [48].

Landing gears are in most cases part of the main air frame however, this is not true for all cases. Landing gears act as the main support for the air frame that bears the load of the overall quadcopter when on ground and especially on landing. As with air frames, landing gears come in wide variety of types and are made of different materials depending on the application [49].

Propellers generate the thrust required for the quadcopter in order to generate the propulsion required to lift the quadcopter and further maneuver it. In propellers

three main components are the material of the propeller, the pitch, and the size of the propeller. The material is mainly determined by the application of the system. While plastic is the most common type of material used for manufacturing propellers. It is not uncommon to find propellers formed by metals and wood as well. The size and the pitch of the propeller determine the overall thrust generated by a propeller. The pitch of a propeller signifies the amount of vertical travel in inches a propeller can achieve by completing one revolution in a soft solid. The size of the propeller determines the overall area the propeller can work on while it rotates [50].

As seen in Figure 3.6 quadcopters consist of four propellers. In order to make sure that the overall moment generated by the quadcopter is zero so that it does not start spinning around its own axis, all quadcopters consist of 2 pairs of propellers. The first pair consist of propellers that generate clockwise moment and the second pair generate anticlockwise moment. In both "+" and "x" configuration a clockwise moving propeller has anticlockwise moving propellers on each side. Figure 3.8 shows a common propeller used in quadcopter.

Figure 3.8: A commonly used 16 x 5.5 inch propeller in quadcopters where 16 is the diameter of the propeller and 5.5 is the pitch of the propeller [51].

3.2.3. Electrical components. The electrical components of a quadcopter consist of 8 main parts. Which are the flight controller, battery, brushless DC mo-

tor, electronic speed controller (ESC), power module, global positioning system (GPS), remote controller (RC) and telemetry. All eight of these are essential electrical components that are required for a basic functional quadcopter.

The flight controller of the quadcopter is the main brain of the system. That includes the control unit of the quadcopter. The flight controller manages all the inputs from the user and the sensors attached to the quadcopter. The flight controller also controls the signals being sent to the motors and thus controls the overall motion of the quadcopter. Most flight controllers also include an inertial measurement unit (IMU) that allows the quadcopter to measure acceleration, rotational velocity and the direction of magnetic field in 3D orientation. This along with other sensors allow the quadcopter to identify its location in a 3D environment. A more detailed analysis on types of flight controllers and their application is provided in [52]. Figure 3.9 shows few of the most commonly used flight controllers used in quadcopters.

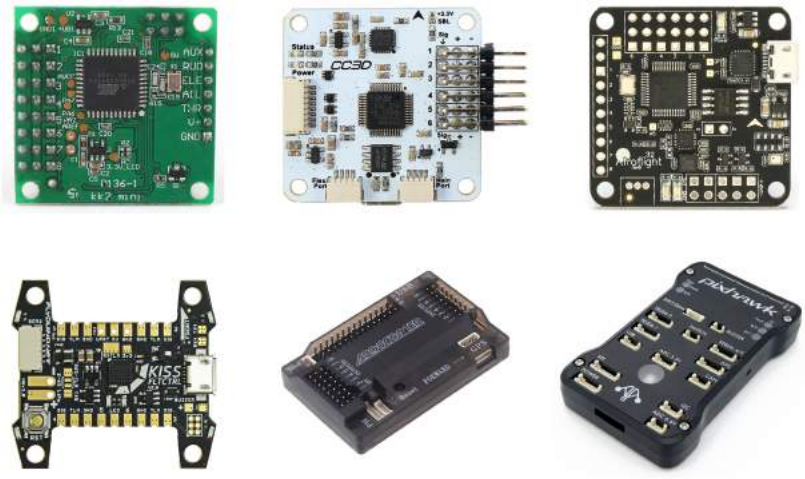

Figure 3.9: Commonly used flight controllers in quadcopters.

Quadcopters can be powered using fuel cells, solar panels and combustion engines [53]. However, the most popular method of powering drones is via batteries and in particular Lithium ion batteries due to their high power density, high voltage per cell, wide temperature operation range, and superior shelf life [2, 54]. A typical Lithium polymer cell has a nominal voltage of around 3.7 volts and are the most prevalent type

of batteries used in quadcopters. These batteries come in a wide variety of size and capacity.

While looking for a Li-Po battery three main things should be kept in mind 1) Battery capacity in mAh, 2) Nominal voltage and 3) Current draw. The nominal voltage is the voltage that the battery provides at full charge. As the charge of the battery decreases so does the voltage provided by the battery. As stated a typical Li-Po battery is rated at 3.7 V. The nominal voltage rating can be increased by connecting two Li-Po batteries with the same current capacity in series with each other. This is typically denoted on Li-Po battery pack as 1S, 2S and so on. Stating the number of cells attached in series in a battery pack. In certain cases where batteries are connected in parallel a number followed by P is shown. A typical combination found on battery case can be 4S1P that sates that the Li-Po in this case have 4 cells that are connected in series and have 1 parallel connection.

The battery capacity in mAh denotes how much current the battery can discharge for in an hour. For example a 1000 mAh battery can provide a load 1 A of current for 1 hour at its nominal voltage. Quadcopters require a large amount of current due to the use of brushless motors (BLDC), as a result general capacities of Li-Po batteries can be anywhere form 2000 mAh to 70000 mAh. It should be evident that the wide range of capacities is to take into account multiple applications that quadcopters have.

BLDC motors require huge amount of current in order to generate the thrust required for the quadcopter. A BLDC motor can take up to 30 A or even more depending on the properties of the BLDC motor. Li-Po battery clearly states the maximum current that can be supplied from the battery by denoting a number followed by C. This is known as the charge and discharge rate of a Li-Po battery and is used to find out the maximum current the battery can provide. For example a battery with 1000 mAh with 20C rating means that the battery can provide a maximum of 20,000 mA (20 A).

Figure 3.10 shows a typical battery used for powering the motors and the electrical components in a quadcopter. The packing shows that this particular battery has a capacity of 1800 mAh at 11.1V (nominal voltage) and a 45C discharge and charge rating.

Figure 3.10: Li-Po battery [55].

Three phase BLDC motors are the main types of motors used in quadcopters. Few key reasons for this is because of their speed/torque characteristic which is almost flat, that allows the motor to operate at the rated load for all speeds. Further advantages of the BLDC motor over DC and AC Induction motors can be found in [56]. One of the most important factors when it comes to quadcopters is the Kv rating which shows the RPM generated by the motor when 1V is applied across it. This rating along with the current draw of the motor helps a user in identifying what type of propellers and ESC are required in order to form an operable quadcopter. Figure 3.11 shows a typical BLDC motor used in quadcopters.

Figure 3.11: A common BLDC motor used in quadcopters [57].

ESCs are the intermediate components that are required to run the brushless DC motor (BLDC). When the user transmits data from the RC the command is received by the flight controller. The flight controller converts the incoming command from the RC to PWM signals. These PWM signals are than fed to the ESC. The ESC then drives the BLDC motor, which drives the propellers, and provides lift to the quadcopter.

ESC in quadcopters are selected based on the maximum current they can provide. ESCs are selected after the motors of the quadcopter have been selected and while not necessary it is always recommended to select an ESC whose maximum current rat-

ing is 10 to 15 A more then the maximum expected current being drawn by the motor. Figure 3.12 shows a common ESC used for building quadcopters.

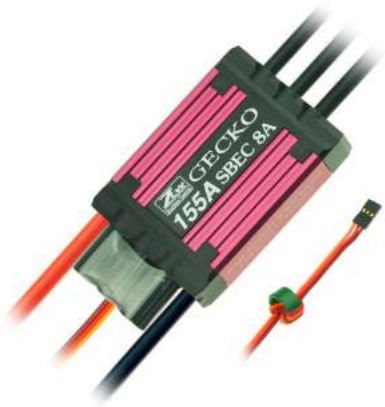

Figure 3.12: A common ESC used in the formation of quadcopters [57].

The power module is a small electrical component that is used to power the flight controller using the Li-Po battery. The power module consists of a voltage converter that converts the voltage level provided from the battery to power the flight controller installed on the quadcopter. The power module also consist of voltage and current sensors that enables monitoring the state of the battery. Figure 3.13 shows a common power module used in a quadcopter.

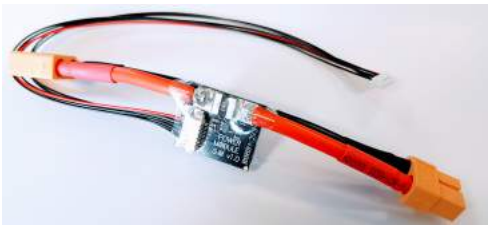

Figure 3.13: A common power module used in the formation of quadcopters [58].

The IMU found in the the flight controller is not enough to localize the quadcopter in an outdoor environment. Almost all drones that are intended to work in outdoor environments have a GPS installed in order to localize the quadcopter. Besides localization one of the most important jobs of GPS is to allow quadcopter to fly autonomously. Figure 3.14 shows a common GPS module used in quadcopter.

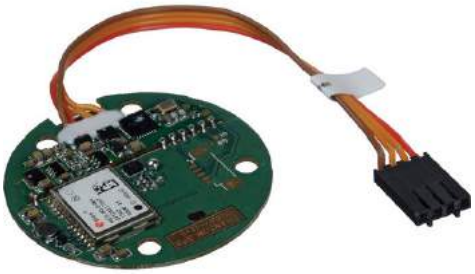

Figure 3.14: A common GPS module used in the formation of quadcopters [59].

In order to manually control the quadcopter a radio transmitter is required. All radio transmitters come with a transmitter and receiver. The transmitter is held by the operator and is used to send commands to the quadcopter. The receiver is connected to the flight controller and the flight controller converts the signal received from the receiver to output on the quadcopter. The most basic quadcopter requires a 6 channel RC transmitter. It is however, common to see RC with 6 channels and above as well. Most RC also operate on a frequency of 2.4 GHz. Figure 3.15 shows a typical RC controller and its receiver used in quadcopters.

Figure 3.15: A common RC transmitter and receiver module used in quadcopters [60].

In order to receive data from the drone while it operating a telemetry module is installed on the drone. The telemetry module comes in two pairs, one is installed on the quadcopter and the second is attached to a computer. Using software such as *QGround-*

Control, *MissionPlanner*, *APM Planner*, the operator can monitor the telemetry data on a computer. The telemetry module not only allows for data observation but can also be used to configure parameters on the quadcopter as well. Since telemetry establishes communication between the user PC (Ground station) it is also used to measure how far it has traveled from its starting point. This particular parameter is used to establish safety precautions. One such safety precaution is to return to home once the connection between the quadcopter and the ground station is broken. Figure 3.16 shows a typical telemetry device used in quadcopters.

Figure 3.16: A common telemetry device used in quadcopters [61].

There are other sensors that can be added to the quadcopter in order to increase its capabilities. A barometric, laser based, or ultrasonic altimeter can help a quadcopter record its altitude in an indoor environment. Similarly a flow sensor can also be attached to a quadcopter in order to measure ground velocity. Gimbals can also be added in order to attach cameras to quadcopter for aerial photography, surveillance, and other similar applications.

3.3. Quadcopter System

While carrying out the literature review on quadcopters based application two common practices were found. In certain cases, research was carried out using custom

built quadcopters, while others use existing out of the box quadcopters and modified them according to their application. Both practices have certain advantages and disadvantages. Custom built drones are highly customizable, and thus the user has the ability to add and remove components without much problems. However, one of the major problems in forming customized quadcopters is that a lot of time has to be invested in calibrating them. Furthermore, before forming the drone, the user also needs to carry out extensive research on the hardware required to form the quadcopter, and also the compatibility of the hardware with other hardware components.

The advantages of using a preassembled quadcopter is that the manufacturer has already taken care of the hardware compatibility of the quadcopter and has already calibrated the system so that it is ready to fly out of the box. Moreover, manufacturers can provide support to the user in case the user faces problems in operating the quadcopter. However, one of the major drawback of an out of the box quadcopter system is its customizability which is usually limited. Nonetheless, out of the box quadcopters are usually intended for applications based research, where the end user would like to focus on applications using the quadcopter and, thus save time on building and calibrating the quadcopter.

For this thesis, an out of the box quadcopter called *Gapter* from *GaiTech EDU* was used. This particular quadcopter was selected due to the onboard computer and its support of robot operating system (ROS). ROS has an open source community that develops ready to use packages that can be installed on a computer and used instantly. This helps users in overcoming cumbersome tasks of developing code and algorithms in order to extract information form a particular hardware device. Proper use of ROS can allow a user to extract essential information from the quadcopter to a ground station running ROS without a lot of configuration software configuration.The support of ROS on Matlab was another reason this particular quadcopter was selected, as this allowed seamless integration of the quadcopter with the ground station running the image processing algorithm. The onboard computer also allows for a USB camera to be attached to the quadcopter. The Gapter specifications are shown in Table 3.2, and the overall hardware connections of the quadcopter is shown in the Figure 3.18 while Figure 3.17 shows how an out of the box Gapter looks like.

Table 3.2: Hardware and Software components of the Gapter.

	Part	**Description**
Hardware	Dimensions	450 mm
	Frame	Carbon Fiber and 3D printed (Acrylonitrile Butadiene Styrene material)
	Weight	Expected to be around 1.7 kg with 4S battery
	Type	X-Quad
	Propellers	9.45
	Color	Black
	Battery	Li-Po
Autopilot Platform	Flight Controller	Pixhawk 2
	Flight Stack	Adrupilot APM
	Onboard Computer	Odroid XU4 with 2 GHz and Octa core CPUs
	RAM	2 GB
	Internal Sensors	Gyroscope, Barometer and 3D accelerometer
	External Sensors	GPS and Optical Flow
	Operating System	Ubuntu 14.04 LTS
	Connectors	1x USB 3.0, and 1x USB 2.0 (dedicated to Wi-Fi USB dongle), HDMI 1.4a for display and Gigabit Ethernet port
	Communication with PC	Wi-Fi and Telemetry

Figure 3.17: A fully assembled out of the box Gapter [62].

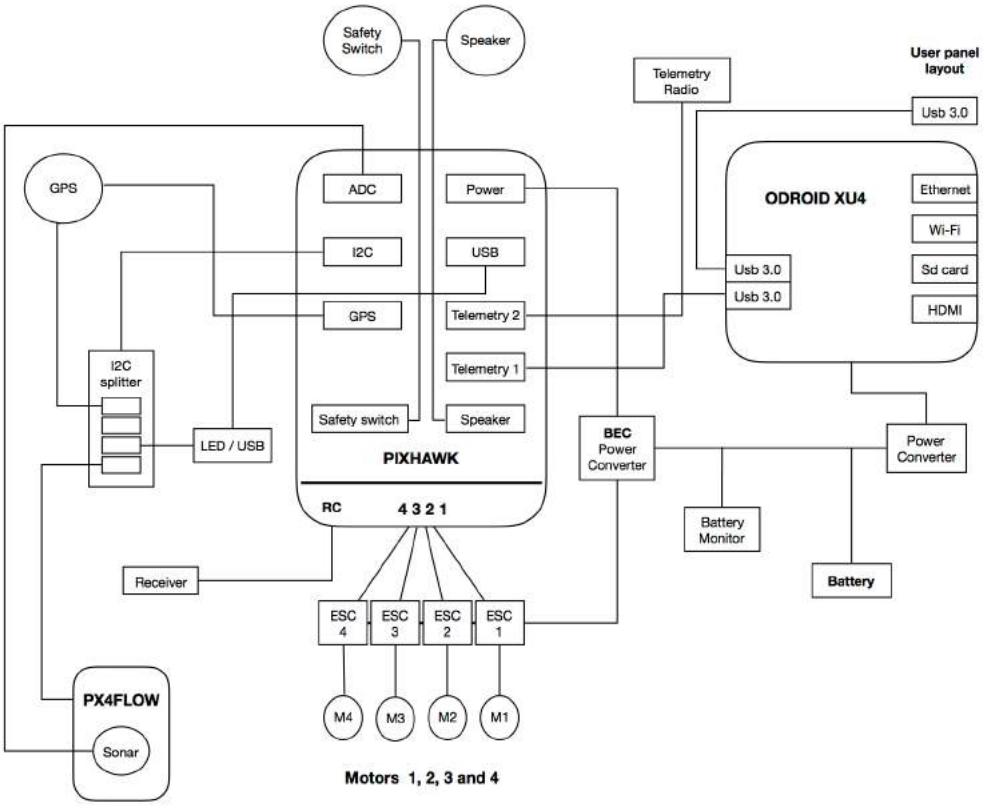

Figure 3.18: Hardware schematic of the Gapter [62].

The major modifications made to the Gapter are the addition of a Raspberry Pi placed at the top of the Gapter with a USB camera and an external power source attached to it. Another separate camera was attached to the Odroid in order to perform off shore image processing. Although the Odroid present on the Gapter has the capability of performing image processing. The software present on the Odroid is not compatible with image processing algorithms built using tensorflow. Therefore an additional computer was installed on the Gapter in order to perform the image processing required.

In addition to this foam legs and a foam platform is also attached to the existing legs of the drone in order to protect the main body from getting damaged in case of rough landings. Furthermore, propeller guards were also attached to each arm in order to protect the propellers from breaking in case of a crash. The final version of the Gapter with all the modifications is shown in Figure 3.19.

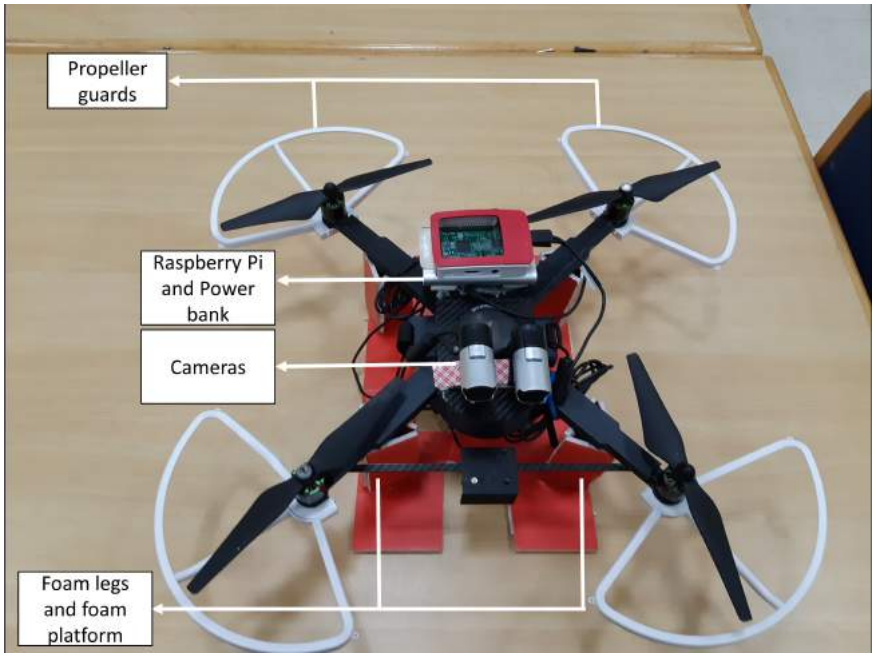

Figure 3.19: Modified Gapter used for insulator detection.

3.4. Overall Quadcopter Based Insulator Health Classification Process

With the image processing algorithms and the overall quadcopter system ready, actual testing of insulator health classification can now be carried out. The overall system works in the following way. 1) The user first calibrates the Gapter using an autopilot software suite and makes sure that the Gapter is in operable condition. 2) The user then initiates ROS on the Gapter and starts publishing GPS coordinates and images from the Gapter. 3) The user then setups the Raspberry Pi on the Gapter and makes sure that the image processing algorithm is running on it. 4) The user then sets up the ground control station to receive images from both the Raspberry Pi and the Odroid. 5) The images from the Odroid are used for offshore processing and are essentially being processed on the ground station; the images from the Raspberry Pi are for onboard real-time classification of insulator health 6) The user then maneuvers the quadcopter to the area where the inspection needs to be carried out. 7) Once the inspection is completed the user can then lands the Gapter and turns it off. 8) The user can then goes through the data by himself from the ground station as well as the onboard data by either accessing the Raspberry Pi remotely or by retrieving the memory stick present on the Pi. Figure

3.20 provides a visual representation of the communication being carried out while the Gapter carries out an inspection.

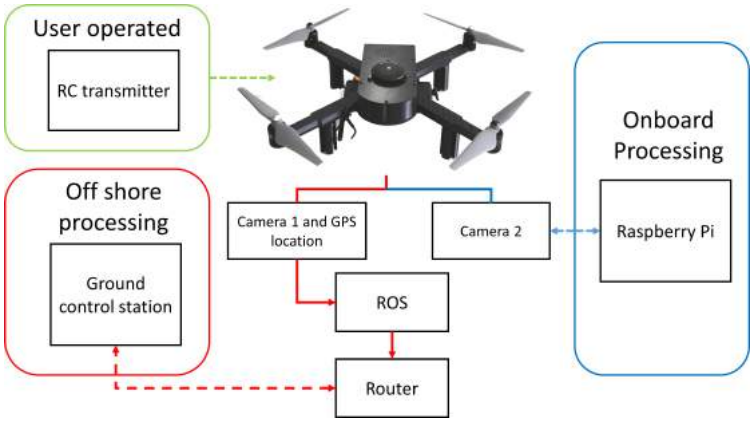

Figure 3.20: A summary of the overall processes being carried out while the Gapter inspects the insulators.

3.5. Hardware Specification

The hardware and software specifications have already been provided for the Gapter. It is however, essential to know the specifications of the other necessary equipment used in this particular thesis.

3.5.1. Ground station. The ground station used for this particular thesis is an **ASUS-GL553VD** laptop. Its specifications are shown in Table 3.3. While not compulsory it has been highly recommended to carry out training and image processing on PC's that have a GPU on it.

Table 3.3: Hardware and software specification of the ground station.

Component	Specifications
CPU	Intel Core -i7-770HQ @ 2.80 GHz
CPU threads	8
RAM	12 GB DDR4
GPU	NVIDIA GeForce GTX 1050
GPU Memory	4 GB
Operating system	Windows 10
Image processing software	Matlab R2018b
Autopilot software suite	QGroundControl

3.5.2. Raspberry Pi . A **Raspberry Pi 3 model B** was used in order to carry out on board image processing. The specification of a typical Raspberry Pi 3 model B are shown in Table 3.4.

Table 3.4: Hardware and software specification of Raspberry Pi 3 model B.

Component	Specifications
System on Chip	BCM2837
CPU	Quad Cortex A 53 @ 1.2 GHz
RAM	1 GB SDRAM
GPU	400 MHz VideoCore IV
Operating system	Raspbian
Image processing software	Tensorflow

3.5.3. Cameras. Two types of cameras were used on the Gapter. The two seen in Figure 3.19 are called **LifeCam Studio Model Q2F-00013** [63], these cameras provide good quality images and were used for both on board and offshore image processing. Detailed specifications of the camera can be found in [63]. In initial testing a low resolution camera was used called **Wei Xn Vision WX071** the specification for this particular camera can be found in [64]. Figure 3.21 shows both cameras that were used in the image acquisition processes.

Figure 3.21: Types of cameras: left WX071 right Q2F-00013.

Chapter 4: Experiments and Results

This chapter primarily focuses on the results obtained from the quadcopter while carrying out insulator inspection. This chapter is divided into further subsections where different scenarios of tests and results are provided. For each test the number of images is provided along with mean average precision (mAP) , average processing time (APT) and other important information.

Before providing the image processing results it is important to understand how to evaluate its performance.This thesis is using a measure called mAP which is obtained by finding the area under a precision-recall curve. In image processing, precision is defined as the number of true positives (T_p) over the number of true positives plus the number of false positives (F_p) Eq (1). Recall on the other hand is defined as the number of T_p over the number of T_p plus the number of false negatives (F_n) Eq (2). The average precision of a particular label is calculated using the maximum precision obtained over 11 segmented recalled values from 0 to 1 in intervals of 0.1 Eq (3).

$$P = \frac{T_p}{T_p + F_p} \tag{1}$$

$$R = \frac{T_p}{T_p + F_n} \tag{2}$$

$$AP = \frac{1}{11} \sum_{r \in (0,0.1....)} p_{interp}(r) \tag{3}$$

For a particular image processing algorithm each label has its own precision-recall curve the mAP is an average precision of all the labels which can be detected by the image processing algorithm. It is also important to understand the key terminologies of T_p, T_n, F_p and F_n. T_p- a true positive occurs when the object detected is present in a given image and its location in the image is also detected correctly. T_n- a true negative occurs when the object is not present in the image and is not detected as well. F_p- a false positive occurs when the object is detected in given image but is not present in it. F_n- a false negative occurs when an object is not detected in given image but is present in it.

In order to calculate the precision-recall curve, tests need to be carried out and then the image processing results need to be compared with the raw images. This is done by labeling the images from the results in order to form the ground truth. As mentioned T_p occur when an object is actually detected and is present in the image. However, one other factor that must be taken into account is how much the detection overlaps with the labeled ground truth. This overlap is determined by the intersection of union (IoU). Which is calculated by using Eq (4). According to [65] an acceptable IoU is 0.5 and above. In this thesis all true positive results occur due to the IoU being 0.5 or greater. In Eq (4) B_p is the area of bounding box that is detected by the algorithm, B_{gt} is the area of the ground truth bounding box.

$$a_o = \frac{area(B_p \cap B_{gt})}{area(B_p \cup B_{gt})} \tag{4}$$

Before discussing details of the results it is important to understand how the offshore and onboard processed images look like and the information they contain. Each information displayed on the image is also saved in a .mat file for offshore processing and .csv file for onboard processing. Figure 4.1 shows two images labeled a and b. The image labeled a is the offshore processed image and the image labeled b is the onboard processed image. 1) shows the date and time the image was processed, 2) shows the detected labels in a given image and the confidence the processing algorithm has on the detection, 3) shows the time taken for the algorithm to processes the image.

(a) (b)

Figure 4.1: Important information from images.

With respect to Figure 4.1 4) is unique to offshore processing and essentially provides GPS coordinates of the quadcopter when the image was taken and processed, 5) is unique to onboard processing and shows the image number. In all eight tests were carried out for insulator inspection and details of each test are provided in Table 4.1. All of the tests mention in Table 4.1 are discussed in detail in this section and readers are encouraged to refer to Table 4.1 if important information regarding a test is missing in its description.

Table 4.1: Insulator inspection test details.

Test no	**Description**	**Offshore or Oboard**	**Distance from over head power line tower**	**Images in data set**
Test 1	Test was carried out on images taken from the trained data set	Offshore	2 m	396
Test 2	Test carried out using WX071	Offshore	Variable between 2 to 3 m	121
Test 3	Test carried out using Q2F-00013	Offshore	Variable between 2 to 3 m	121
Test 4	Test carried out using Q2F-00013	Offshore	Variable between 2 to 3 m	151
Test 5	Test carried out using Q2F-00013	Offshore	Variable between 1 to 2 m	151
Test 6	Test carried out using Q2F-00013	Onboard	Variable between 1 to 2 m	179
Test 7	Test carried out using Q2F-00013	Offshore	Variable between 0.5 to 1 m	151
Test 8	Test carried out using Q2F-00013	Onboard	Variable between 0.5 to 1 m	216

4.1. Test 1: Image Set From Training Environment (Ground Station)

In order to test out the performance of the image processing algorithm, the first test that was carried out was using a small set of 396 images from the training data. This was done in order to check how the algorithm works in an environment that is known to it. The precision recall for each category is shown in Figure 4.2. Figure 4.3, 4.4 and 4.5 show the overlap ratio for each particular category along with instances of T_p, T_n, F_p and F_n. The histograms show overall in the given data set how many images come under each category. Figure 4.6 shows the result obtained after processing the image for insulator detection. In addition to this Table 4.2 summarizes the results for test 1.

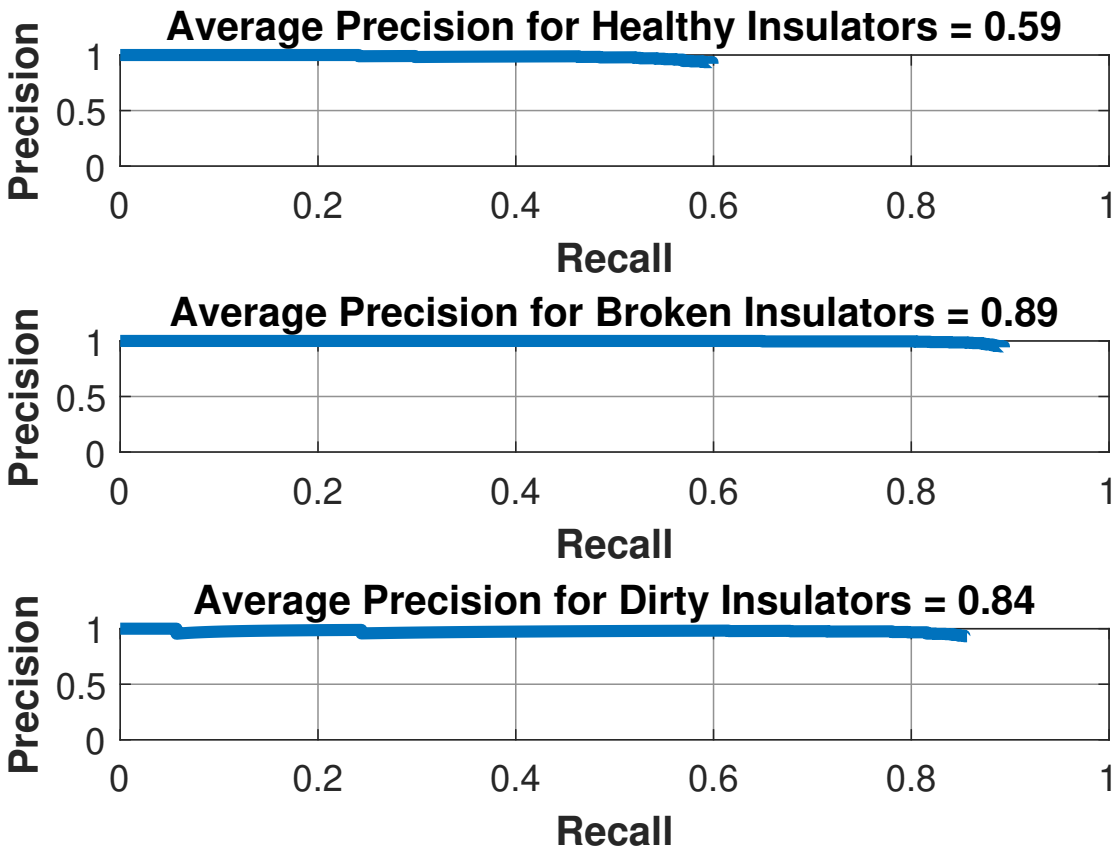

Figure 4.2: Precision-recall curve for all three categories.

In Figure 4.3, 4.4 and 4.5 the black dotted line in the top most graph shows a threshold. This threshold is set at 0.5 which helps in identifying how much overlap occurs when a T_p occurs. As mentioned before, the existence of a label in an image is not enough to categorize the label as T_p. The IoU helps us in identifying when a label

is detected, how much of the detection overlaps with the actual object, which the user has defined. In case the IoU is below the expected value of 0.5 this instance is then categorized as F_p. Another important point is the appearance of T_n instances. While T_n are not used in calculation they are important. This is because a T_n represents instances where a result is not expected, and the algorithm also does not provide any output.

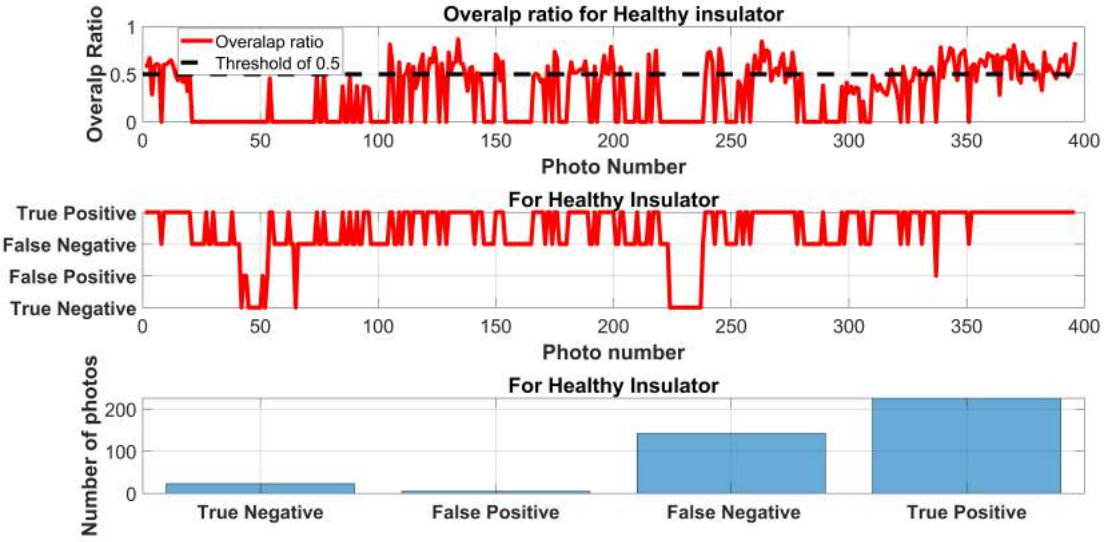

Figure 4.3: Test 1 overlap ratio and overall processing result for healthy insulators.

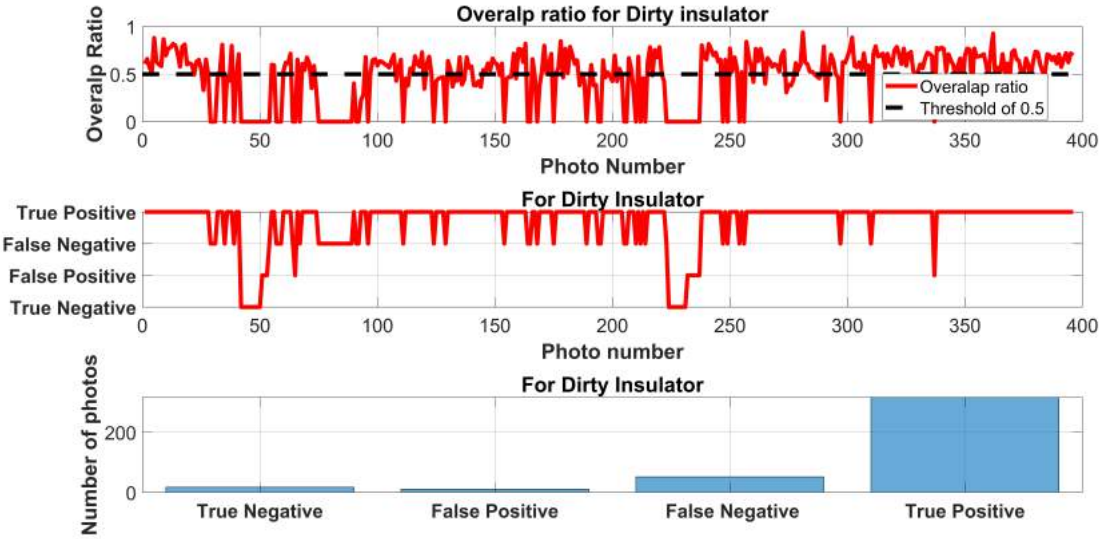

Figure 4.4: Test 1 overlap ratio and overall processing result for dirty insulators.

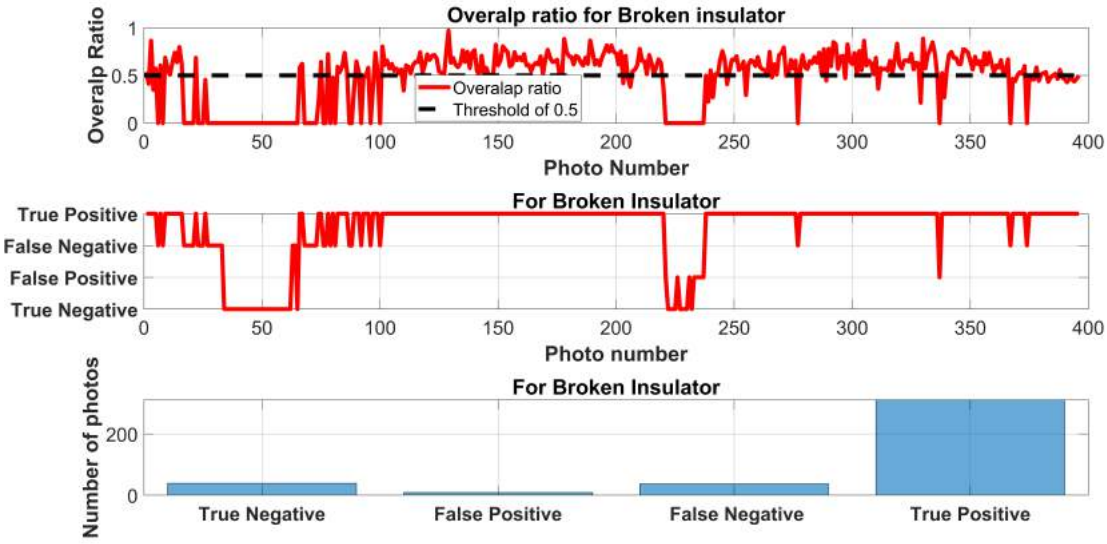

Figure 4.5: Test 1 overlap ratio and overall processing result for broken insulators.

Figure 4.6: Result of image number 15 from test 1 image data set.

Table 4.2: Data from insulator inspection test 1.

Attribute	**Value**
AP Healthy	0.59
AP Broken	0.89
AP Dirty	0.84
Average overlap ratio (Healthy)	0.55
Average overlap ratio (Broken)	0.61
Average overlap ratio (Dirty)	0.61
mAP	0.77
APT	0.44 seconds

Form values in Table 4.2 and the graphs above, the overall performance of the test can be evaluated. AP Healthy is the lowest among all three categories by referring to Figure 4.2 it can be observed that the AP value is low due to the low recall value which means that there is a presence of a large number of F_n values. However, what is promising is that the precision of the system is still considerably high for healthy insulators. With regards to the other two label dirty and broken the algorthim performed quite well as AP for broken is 0.89 and AP for dirty is 0.84 which means that algorithm has both high precision and recall for these particular labels which can be further verified by Figure 4.2. The mAP for all three categories is 0.77 which is acceptable. The major factor however is the APT value which is 0.44 seconds on the ground station. This means that real time monitoring of insulators can be conducted on this system with relatively quick response. Average overlap ratio helps us identify that overall when a T_p instance does occur it mostly overlaps the expected ground truth region.

Results obtained from test 1 were promising and while AP for healthy insulators was quite low in comparison to dirty and broken insulators. It was still decided to carry forward with CIFAR-10 based RCNN system because of its speed and also because while testing it was expected that multiple images will be taken of the same pole while carrying out inspection. The algorithms high precision capability in all three labels means that if multiple images are taken near a single overhead power line tower, then there are chances of detecting all insulators present on the line and their health.

4.2. Test 2: Insulator Inspection Via Quadcopter (Ground Station)

Test 2 was carried out using the lower quality WX071 camera. Since the gapter came with WX071 it was used with the Gapter for initial tests. Results form test 2 showed that the performance of the algorithm with a lower quality camera is not good but this instead was used in order to understand the image quality requirements that the algorithm needs in order to provide better results. Figure 4.7 shows the map location where the test was carried out while Figure 4.8 shows the precision-recall curve for test 2. Figure 4.9, 4.10 and 4.11 show the overall results for all three categories and Figure 4.12 shows few processed images from test 2.In addition to this Table 4.3 summarizes the results for test 2.

The red cross in Figure 4.7 show the take off and landing point of the quadcopter once the inspection is complete. The blue arrows show the direction in which the quadcopter will move in order to carry out the inspection. and the white arrow shows the location of the tower which is being inspected.

Figure 4.7: Location where test 2 was carried out on a map.

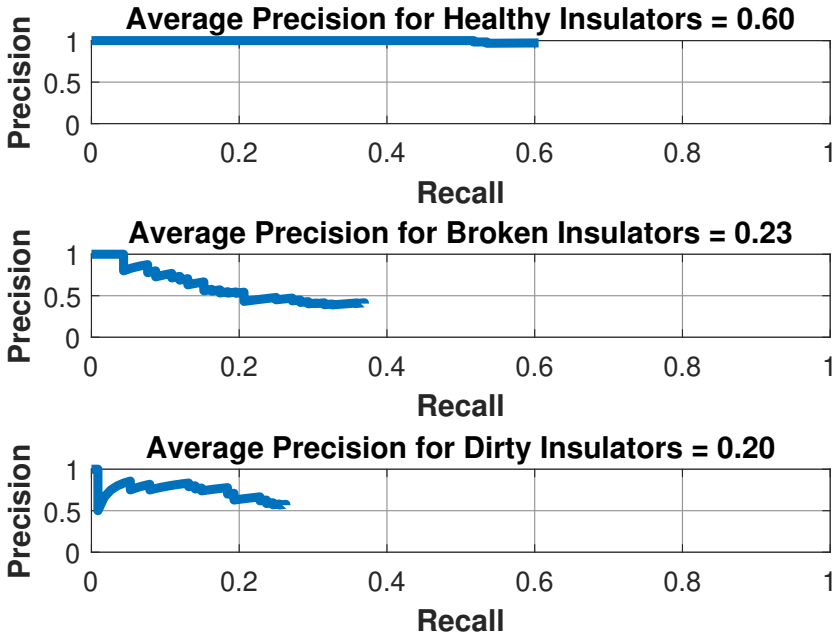

Figure 4.8: Precision-recall curve for all three categories for test2.

Similar to Figures 4.3, 4.4 and 4.5, Figures 4.9, 4.10 show instances of T_p, T_n, F_p and F_n. Furthermore, the threshold is also present at 0.5. The results of these three Figures are not similar to the ones observed in Figure 4.3, 4.4 and 4.5. Besides, in Figure 4.9 the instances of F_n are considerably higher for broken and dirty insulators. This means that the overall recall for these two label is low and this is observed in Figure 4.8.

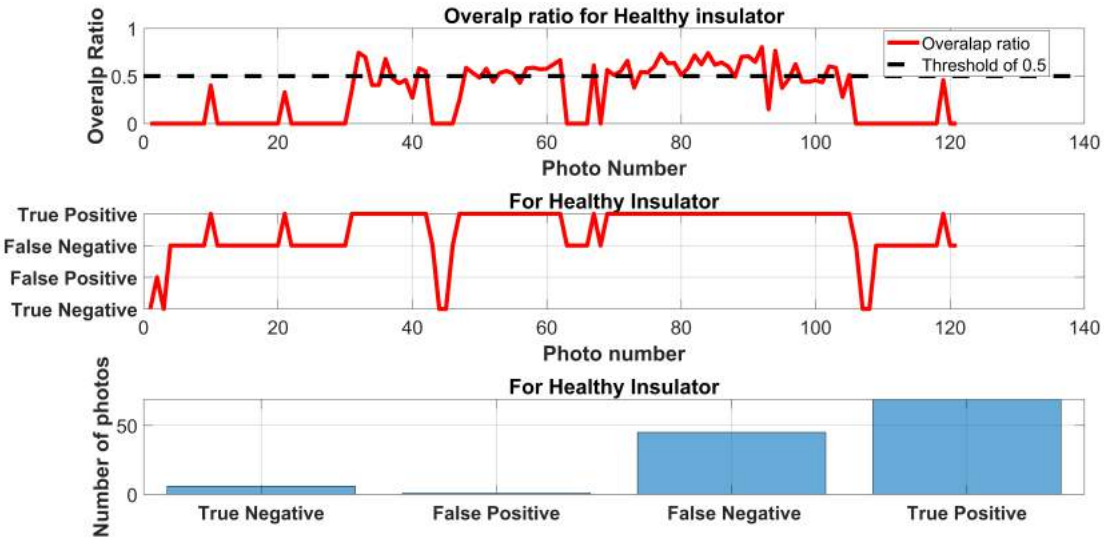

Figure 4.9: Test 2 overlap ratio and overall processing result for healthy insulators.

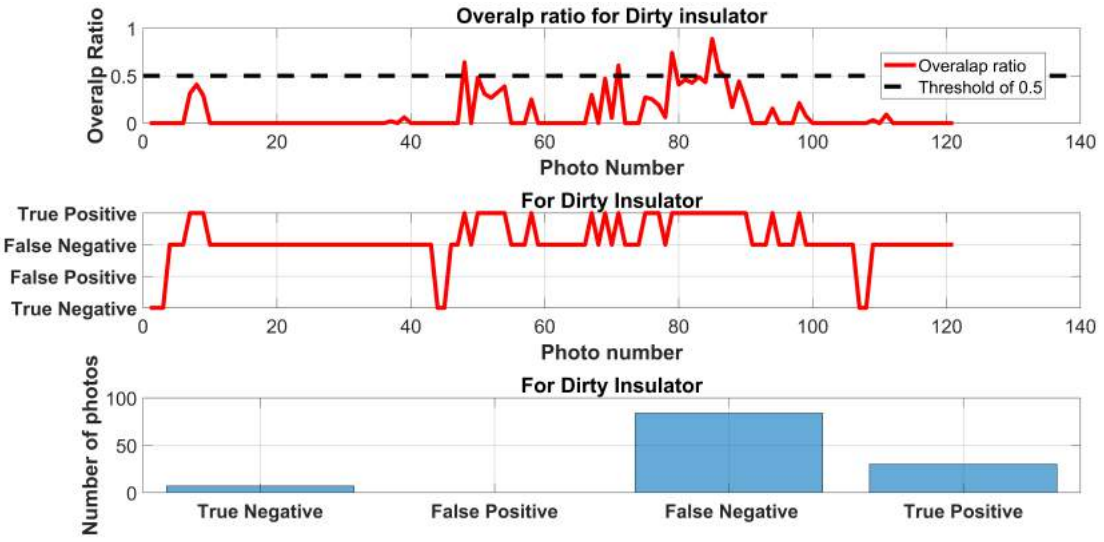

Figure 4.10: Test 2 overlap ratio and overall processing result for dirty insulators.

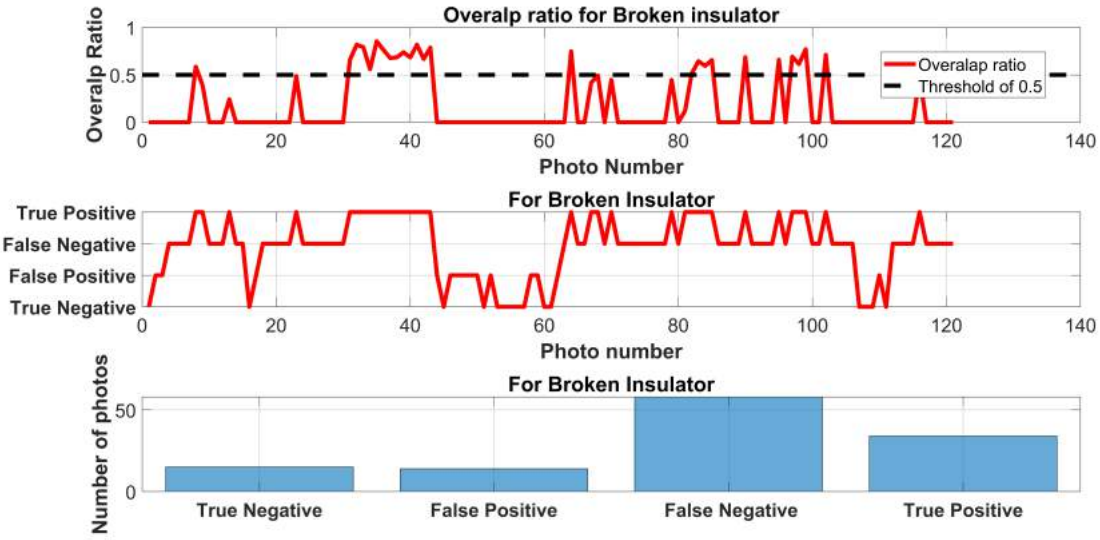

Figure 4.11: Test 2 overlap ratio and overall processing result for broken insulators.

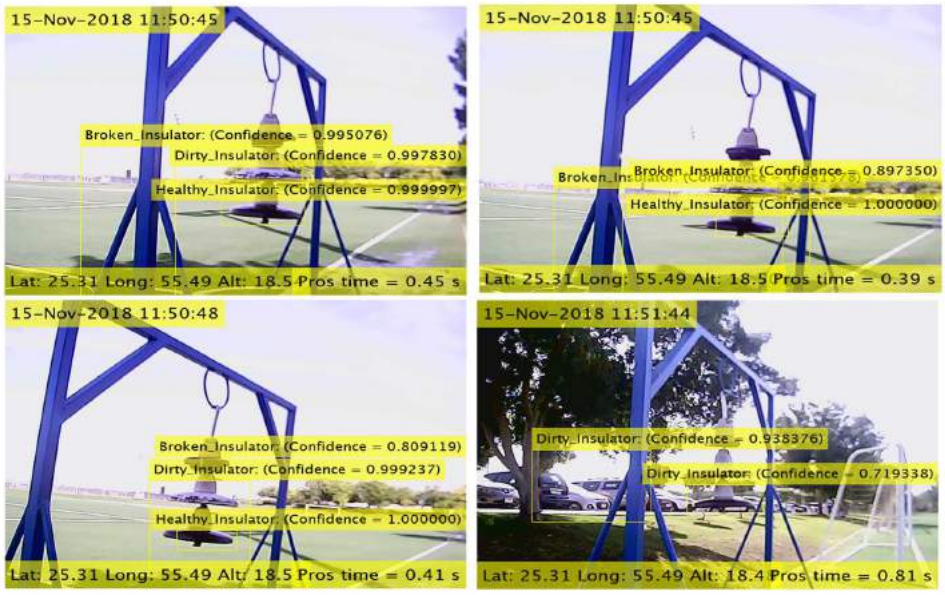

Figure 4.12: Four images from the overall 121 images that were processed from test 2.

Overall 121 images were captured in test 2 while flying the quadcopter. While not clear in the images shown in Figure 4.12 the quality of the images when observed individually were not good. Comparisons between broken and dirty insulators was difficult to make and this is further supported by the fact that the occurrences of F_p for

broken insulators is high. As in certain photos, the dirty insulator is marked as a broken insulator.

Table 4.3: Data from insulator inspection test 2.

Attribute	Value
AP Healthy	0.60
AP Broken	0.23
AP Dirty	0.20
Average overlap ratio (Healthy)	0.53
Average overlap ratio (Broken)	0.60
Average overlap ratio (Dirty)	0.32
mAP	0.34
APT	0.55 seconds

The results above show that the quality of the camera greatly affects the detection algorithm. The AP values for all three categories is considerably less then the values obtained from test 1. As a result mAP is also lower than the one observed in test 1. The major problem noticed is the lack of quality of the image, it was noticed that the brightness, contrast and overall image quality was not good, and as a result the algorithm performance is not good.

4.3. Test 3: Insulator Inspection Via Quadcopter (Ground Station)

This particular test was carried out using the Q2F-00013 camera. To test out if changing the cameras provided improvements in the AP for each category, this test only used offshore processing. One considerable major change that was made was that in this particular test two different overhead towers were used. Figure 4.13 shows the two overhead towers used for this test. Figure 4.14 shows the location where the test was carried out while Figure 4.15 shows the precision-recall curve for all three labels for test 3. Figure 4.16, 4.17 and 4.19 show the overall results for all three categories. In addition to this Table 4.4 summarizes the results for test 3. Note: test 3 to 8 were carried out close to the vicinity shown in Figure 4.14 therefore for further test the map location is not shown and readers can refer to Figure 4.14 for the map location.

The red cross in Figure 4.14 show the take off and landing point of the quadcopter once the inspection is complete. The blue arrows show the direction in which the quadcopter will move in order to carry out the inspection. and the white arrows shows the location tower 1 and tower 2 which are being inspected.

Figure 4.13: Over head towers used in test 3.

Figure 4.14: Location where test 3-8 were carried out on a map.

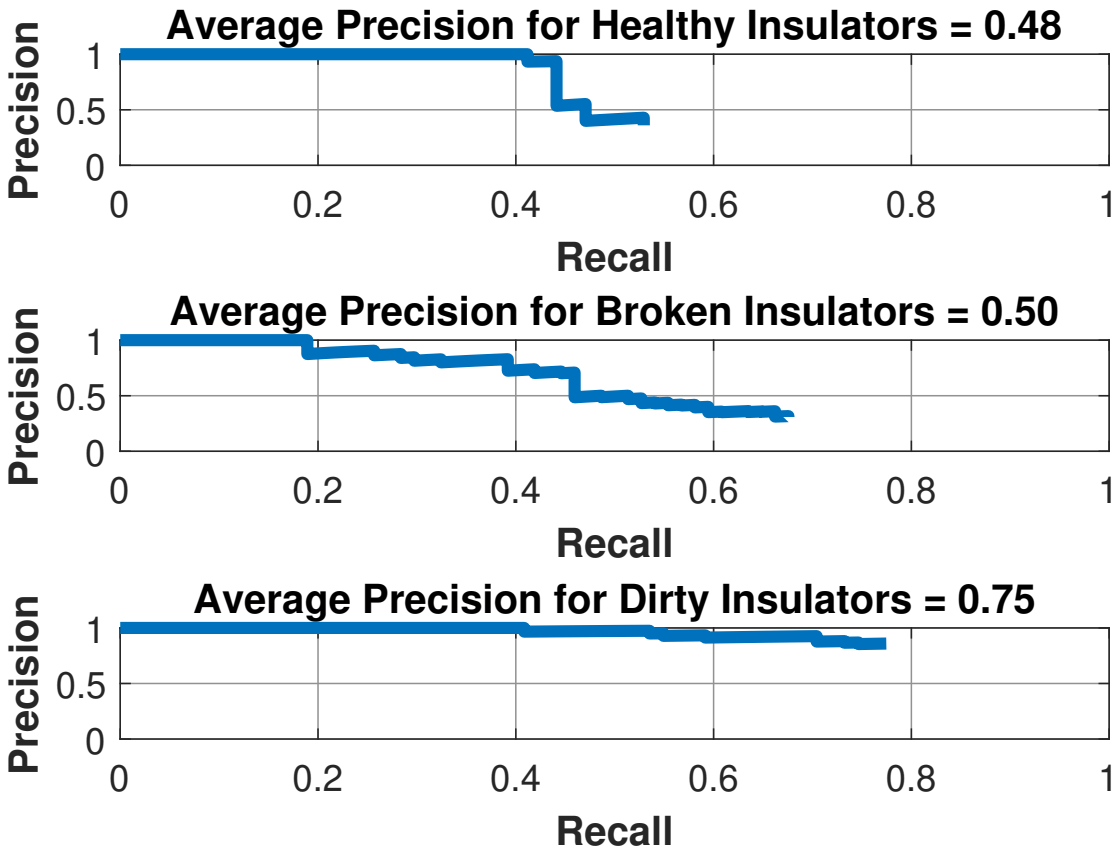

Figure 4.15: Precision-recall curve for all three categories for test 3.

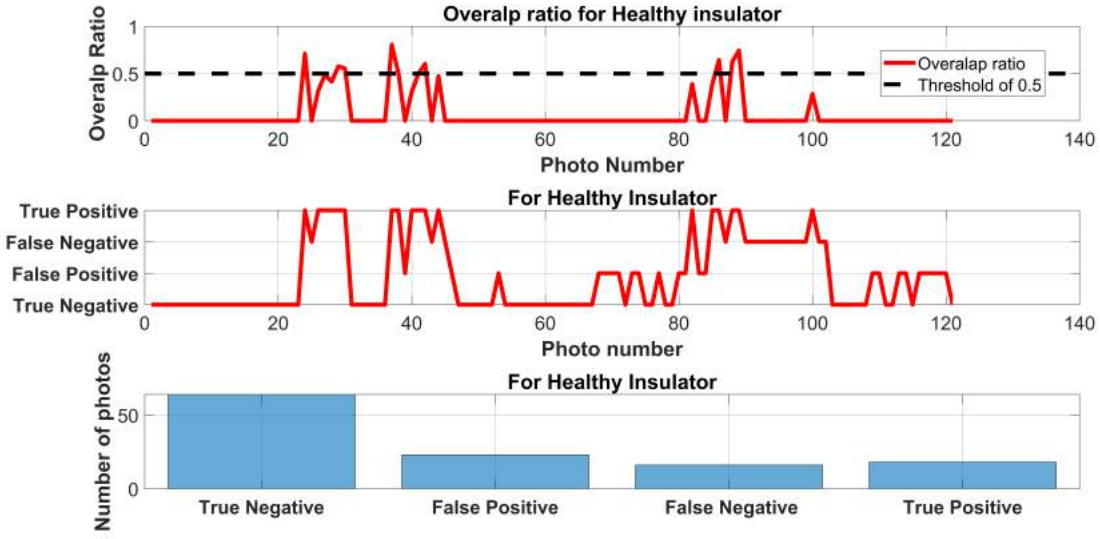

Figure 4.16: Test 3 overlap ratio and overall processing result for healthy insulators.

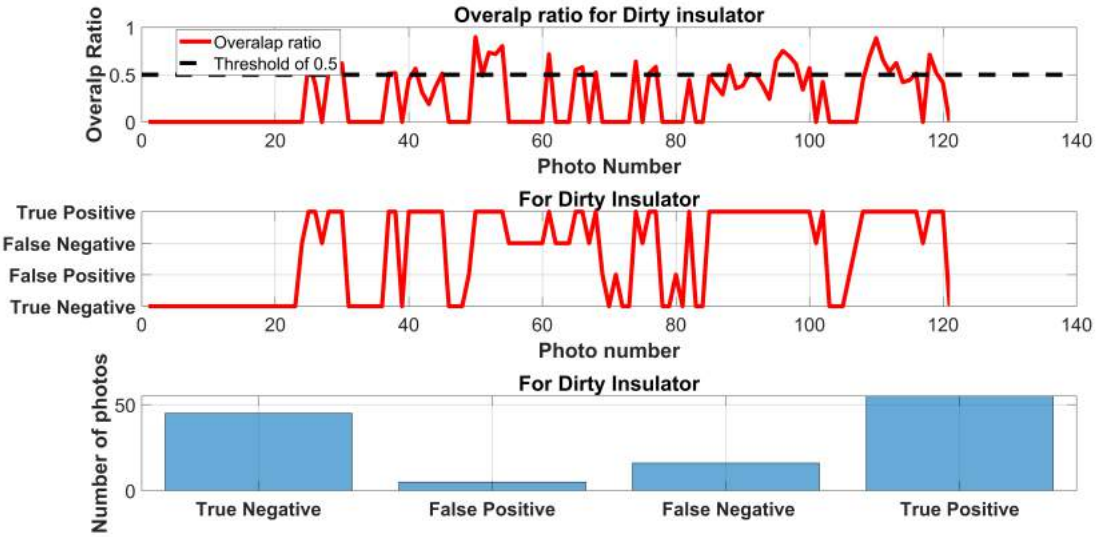

Figure 4.17: Test 3 overlap ratio and overall processing result for dirty insulators.

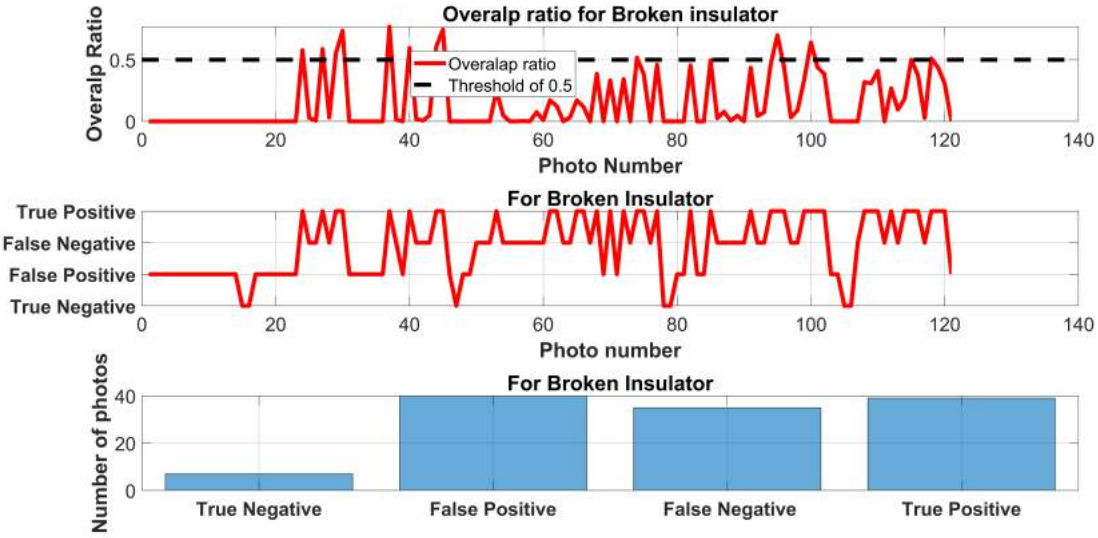

Figure 4.18: Test 3 overlap ratio and overall processing result for broken insulators.

Overall 121 images were captured in test 3 while flying the quadcopter. Out of 121 images few images are shown in Figure 4.19. When compared to previous results this particular test showed that changing the camera had a considerable impact on the detection results. When Figure 4.17, 4.18 and 4.19 are observed it is evident that an improvement in both recall and precision has been made when comparing to similar graphs in test 2.

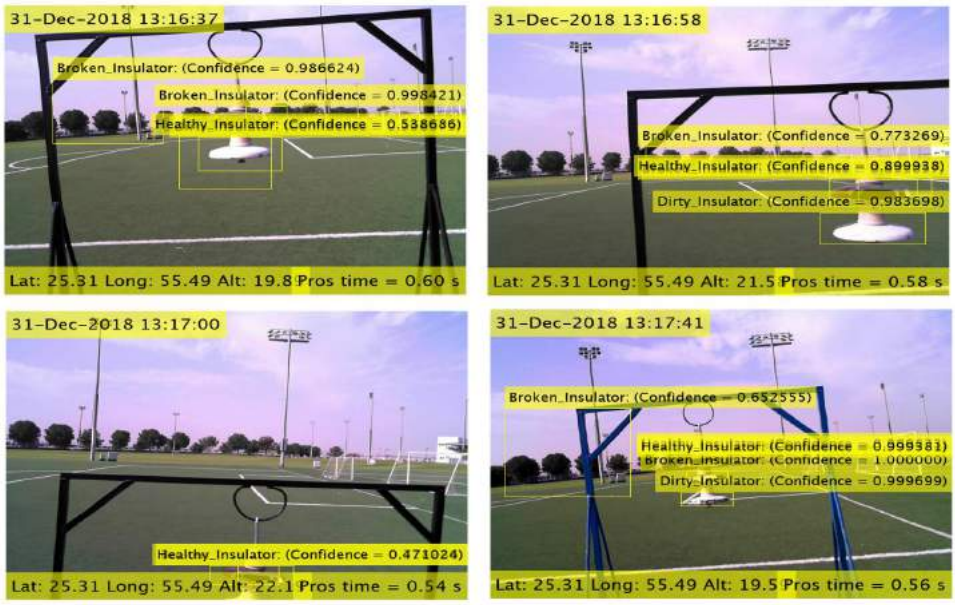

Figure 4.19: Four images from the overall 121 images that were processed from test 3.

Table 4.4: Data from insulator inspection test 3.

Attribute	**Value**
AP Healthy	0.48
AP Broken	0.50
AP Dirty	0.75
Average overlap ratio (Healthy)	0.49
Average overlap ratio (Broken)	0.29
Average overlap ratio (Dirty)	0.52
mAP	0.58
APT	0.52 seconds

Results from test 3 show that changing the camera made significant improvements when it came to detection of broken and dirty insulators as results from Table 4.4 show improvements in AP for broken and dirty insulators when compared to Table 4.3. A concern is the detection of healthy insulator which has not been detected well, as seen by results from Table 4.4 as well as Figure 4.16. It was decided to observe the detection results from future tests and see how the label detection performs in different conditions.

Another major problem that was noticed was the increase in F_n cases in the new data sets after going through the results it was found that the algorithm was giving F_n results with lower level of confidence. An increase in F_n results in an overall decrease in the recall of the label. As a result it was decided to make changes to the algorithm in order to detect results with certain level of threshold. Through experiments with various data sets it was decided to select a score threshold of 0.85. Which meant that a detection is accepted only if the algorithm gave the detection a confidence score of 0.85 or above. This would mean that F_n results will decrease but also cases of T_p will suffer. Discussion on how the threshold was decided are discussed in a latter discussion.

4.4. Test 4: Insulator Inspection Via Quadcopter (Ground Station)

This particular test was carried out using the Q2F-00013 camera. To test different scenarios with the quadcopter. Figure 4.20 shows the precision-recall curve for all three labels for test 4. Figure 4.21, 4.22 and 4.23 show the overall results for all three categories and Figure 4.24 shows 4 processed images from test 4 data set. In addition to this Table 4.5 summarizes the results for test 4.

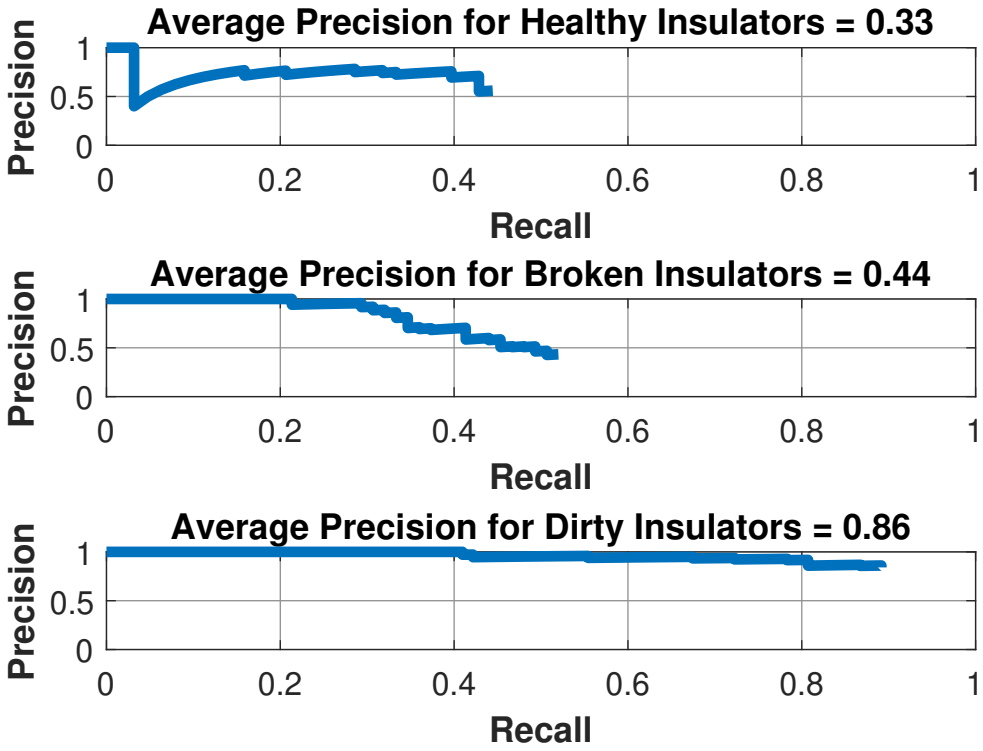

Figure 4.20: Precision-recall curve for all three categories for test 4.

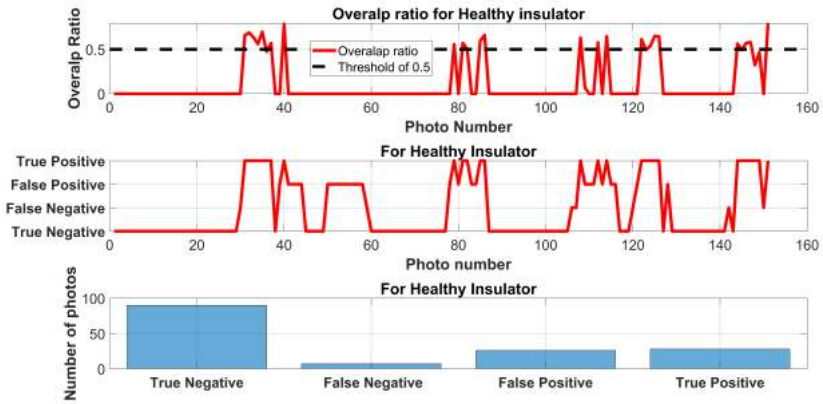

Figure 4.21: Test 4 overlap ratio and overall processing result for healthy insulators.

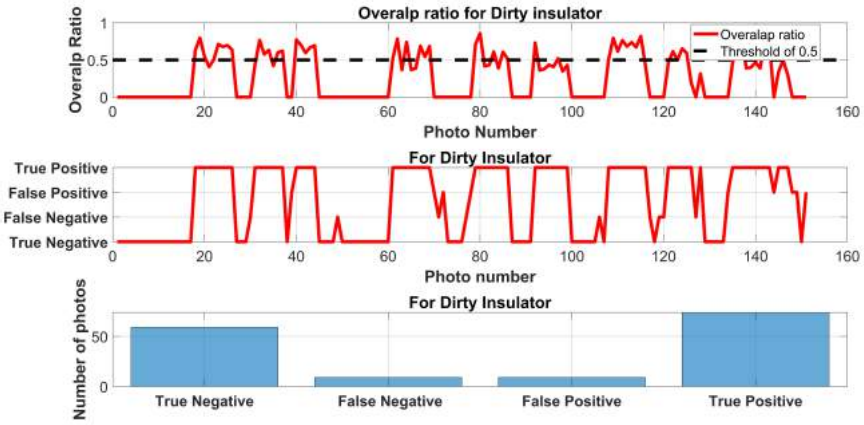

Figure 4.22: Test 4 overlap ratio and overall processing result for dirty insulators.

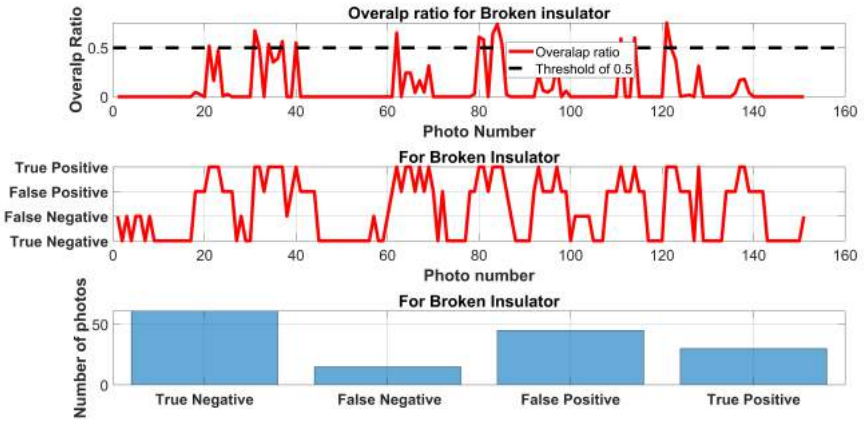

Figure 4.23: Test 4 overlap ratio and overall processing result for broken insulators.

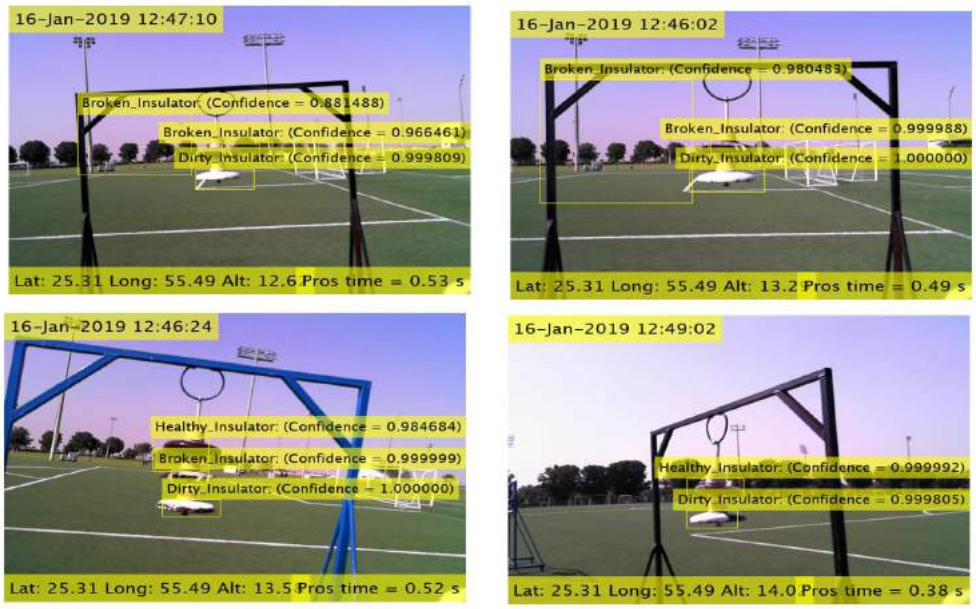

Figure 4.24: Four images from the overall 151 images that were processed from test 4.

Table 4.5: Data from insulator inspection test 4.

Attribute	Value
AP Healthy	0.33
AP Broken	0.44
AP Dirty	0.85
Average overlap ratio (Healthy)	0.55
Average overlap ratio (Broken)	0.29
Average overlap ratio (Dirty)	0.56
mAP	0.54
APT	0.70 seconds

Results from test 4 show that detection of broken and dirty insulators is still better when compared with healthy insulator detection. Ap values for Table 4.5 further confirm the results shown in Figure 4.21, 4.22 and 4.23. With the detection results showing promise it was decided to carry out test for onboard processing as well.

4.5. Test 5: Insulator Inspection Via Quadcopter (Ground Station)

This particular test was carried out using the Q2F-00013 camera. To test different scenarios with the quadcopter. Figure 4.25 shows the precision-recall curve for all

three labels for test 5. Figure 4.26, 4.27 and 4.28 show the overall results for all three categories and Figure 4.29 shows 4 processed images from test 5 data set. In addition to this Table 4.6 summarizes the findings in for test 5.

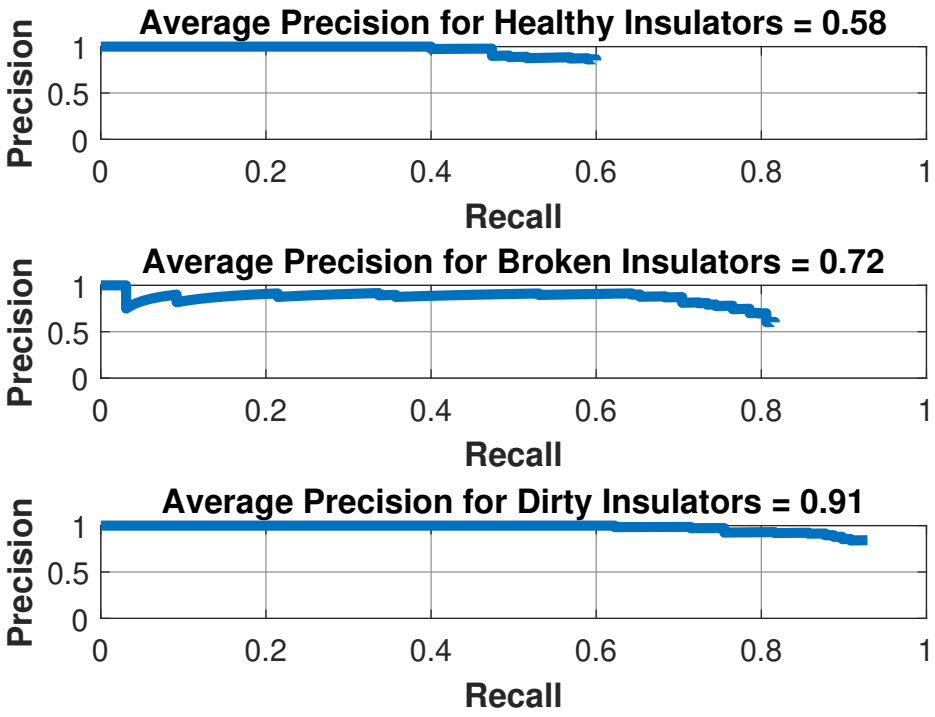

Figure 4.25: Precision-recall curve for all three categories for test 5.

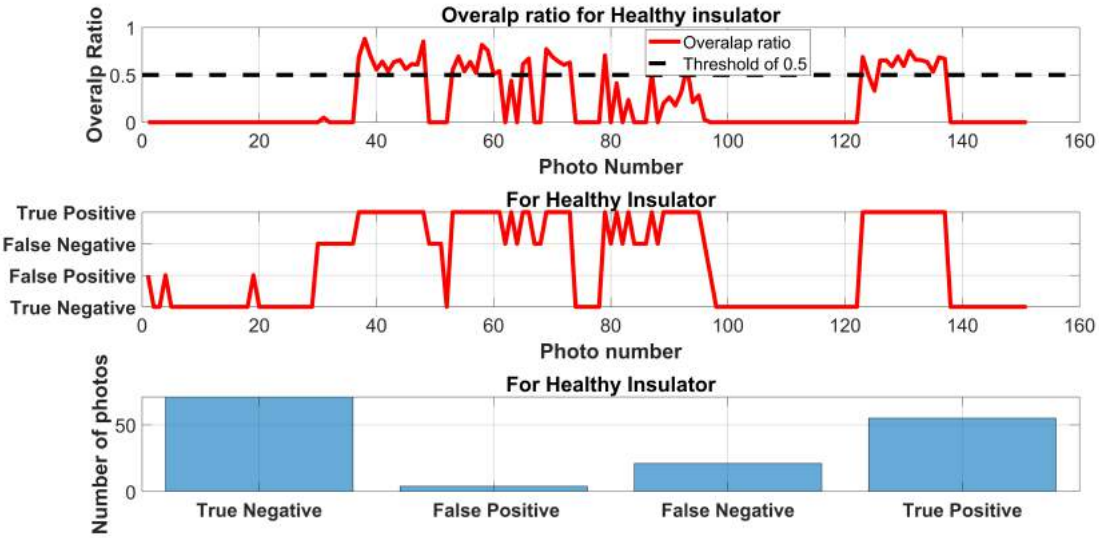

Figure 4.26: Test 5 overlap ratio and overall processing result for healthy insulators.

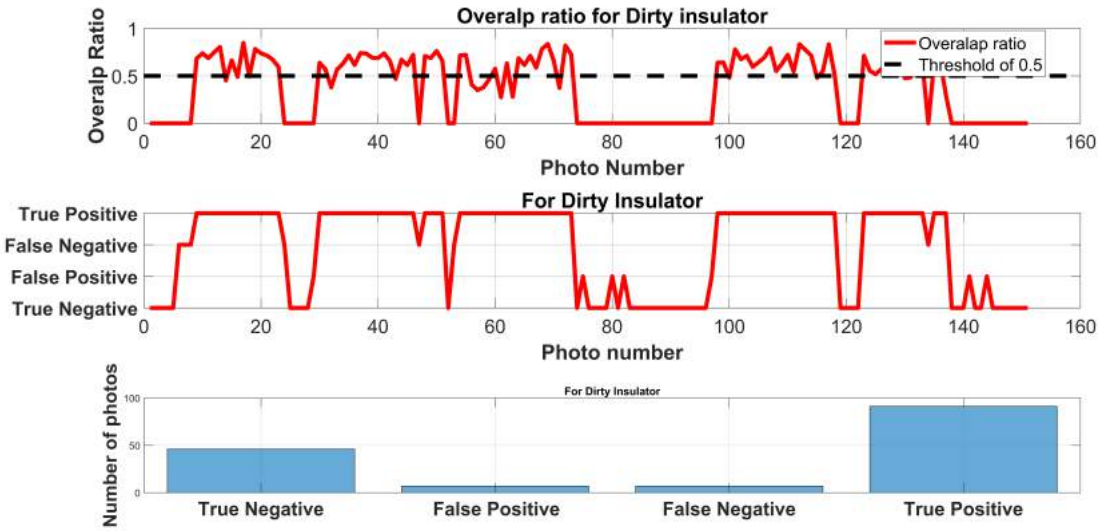

Figure 4.27: Test 5 overlap ratio and overall processing result for dirty insulators

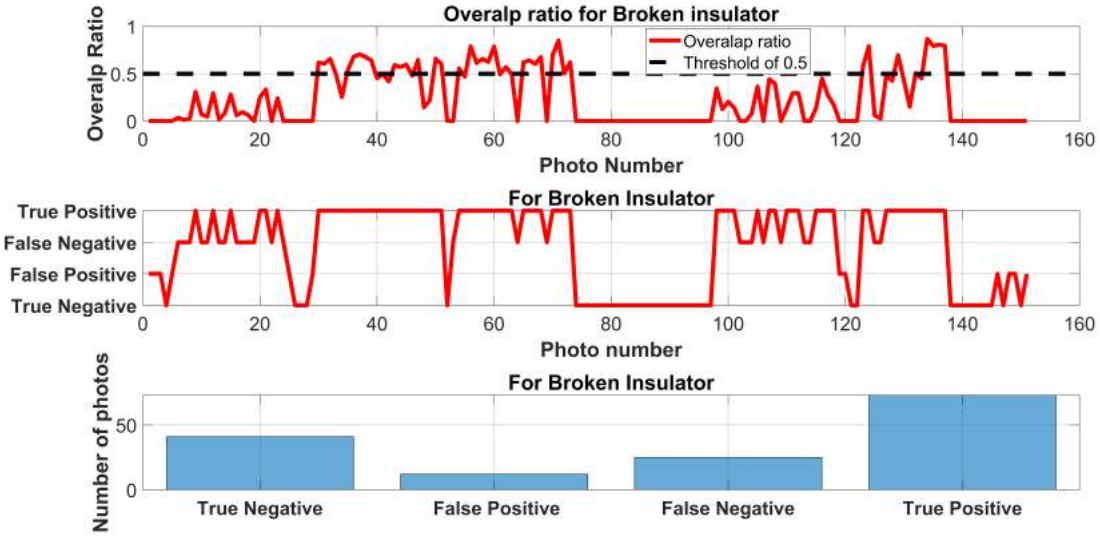

Figure 4.28: Test 5 overlap ratio and overall processing result for broken insulators.

After applying the threshold of 0.85 in test 5 the results obtained show improvements in detection of all three labeled categorizes. With respect to Figures 4.26, 4.27 and 4.28 it can be seen that the instances of F_n have started to decrease and as a result the precision is improving fro all three categories as seen in Figure 4.25. A repeated problem of the recall capability of the healthy insulator is also evident.

Figure 4.29: Four images from the overall 151 images that were processed from test 5.

Table 4.6: Data from insulator inspection test 5.

Attribute	**Value**
AP Healthy	0.58
AP Broken	0.72
AP Dirty	0.91
Average overlap ratio (Healthy)	0.55
Average overlap ratio (Broken)	0.42
Average overlap ratio (Dirty)	0.62
mAP	0.74
APT	0.58 seconds

4.6. Test 6: Insulator Inspection Via Quadcopter (Onboard)

This particular test was carried out using the Q2F-00013 camera. This test was carried out simultaneously with test 5 and the processing was done on the onboard Raspberry Pi. Discussion of this particular test is done in tandem with test 5. Figure 4.30 shows the precision-recall curve for all three labels for test 6. Figure 4.31, 4.32 and 4.33 show the overall results for all three categories and Figure 4.34 shows 4 processed

images from test 6 data set. In addition to this Table 4.7 summarize the findings in for test 6.

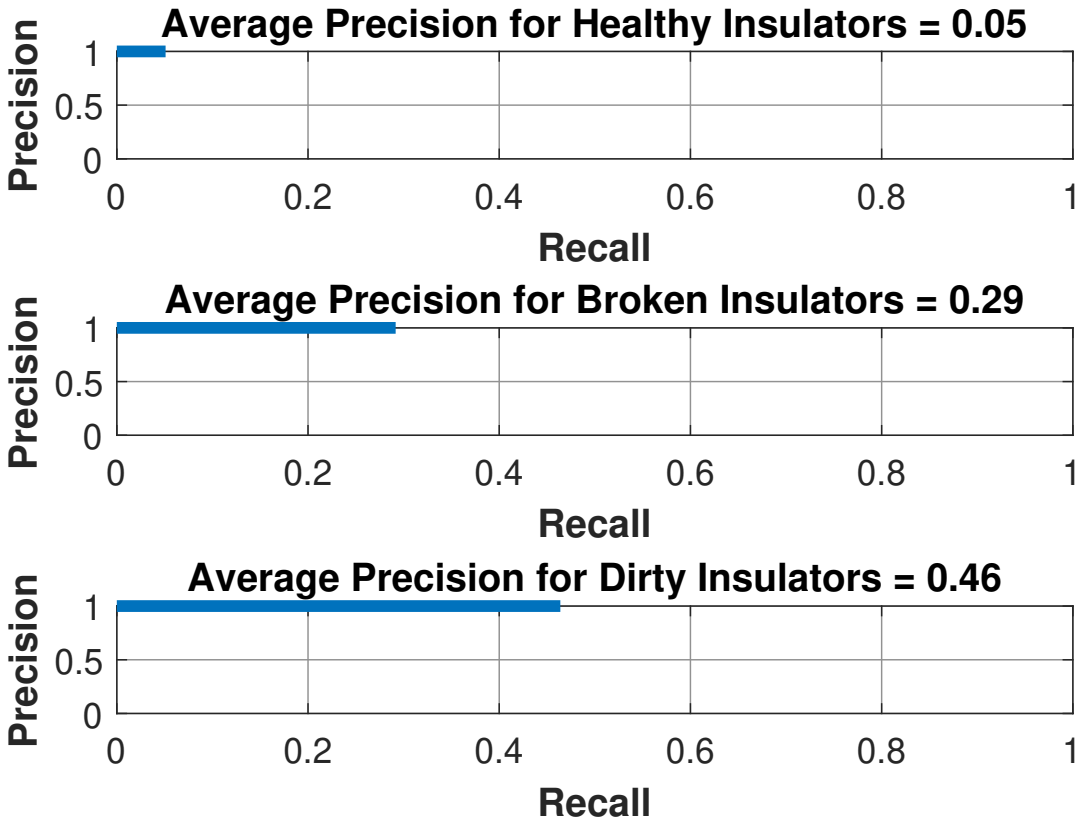

Figure 4.30: Precision-recall curve for all three categories for test 6.

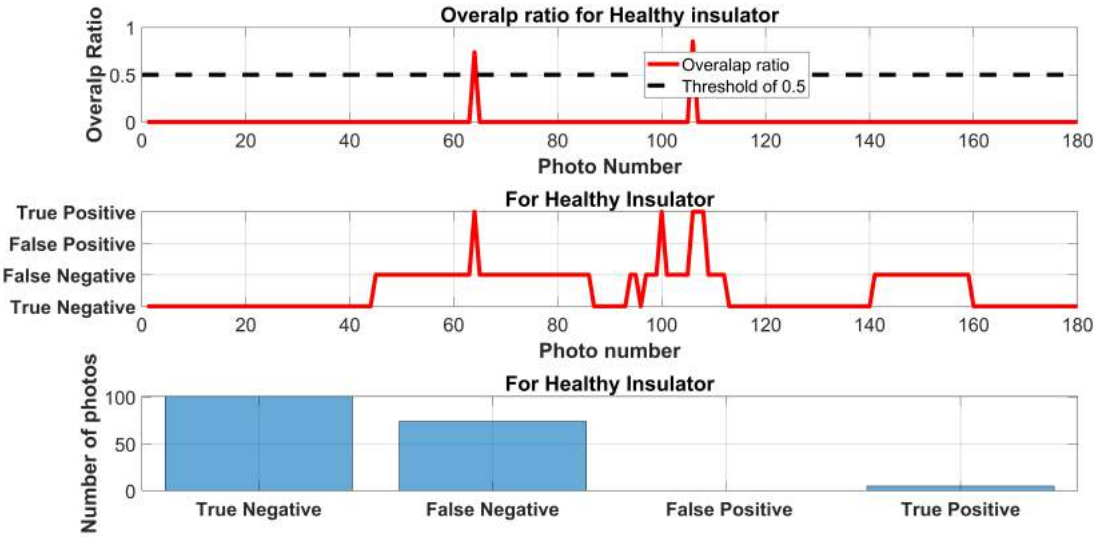

Figure 4.31: Test 6 overlap ratio and overall processing result for healthy insulators.

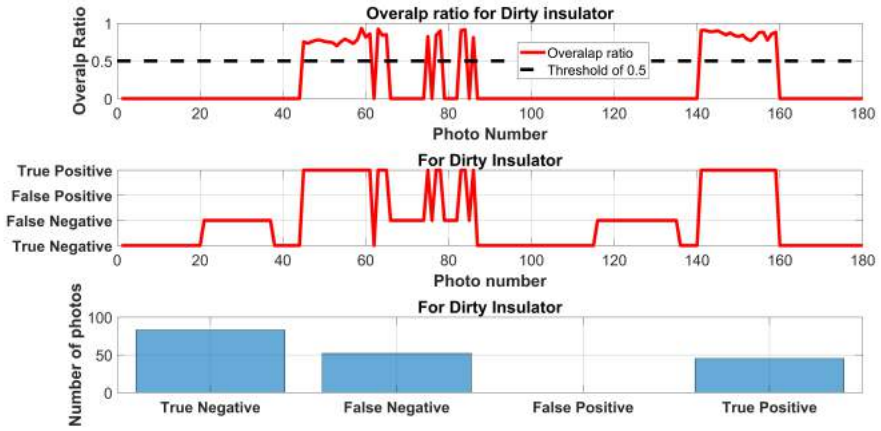

Figure 4.32: Test 6 overlap ratio and overall processing result for dirty insulators.

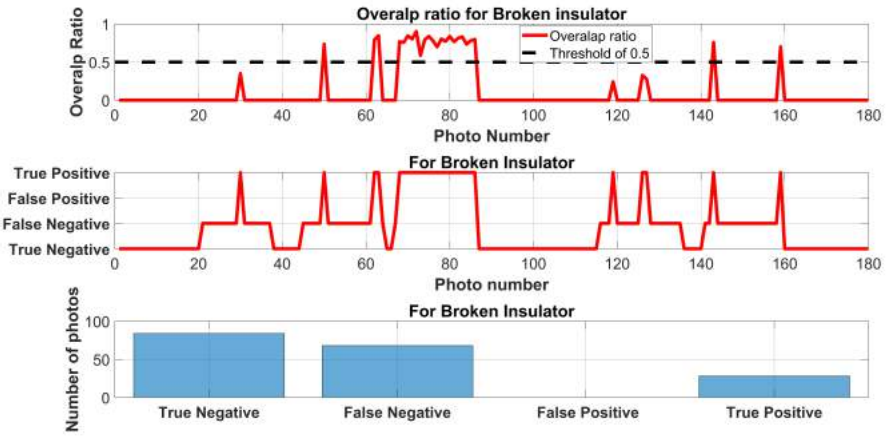

Figure 4.33: Test 6 overlap ratio and overall processing result for broken insulators.

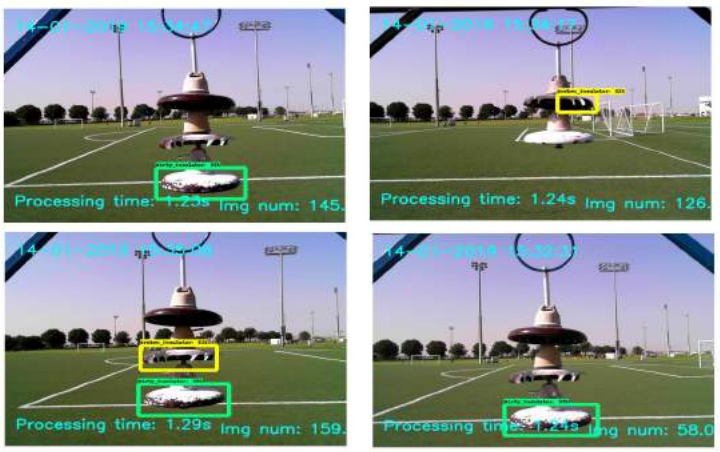

Figure 4.34: Four images from the overall 134 images that were processed from test 6.

Table 4.7: Data from insulator inspection test 6.

Attribute	Value
AP Healthy	0.05
AP Broken	0.29
AP Dirty	0.46
Average overlap ratio (Healthy)	0.53
Average overlap ratio (Broken)	0.69
Average overlap ratio (Dirty)	0.81
mAP	0.27
APT	1.27 seconds

Results obtained from Raspberry Pi are interesting, AP values from Table 4.7 and graphs from Figure 4.30 show that onboard processing is possible. However, recall capability of the algorithm developed for Raspberry Pi is significantly less. Results from Figure 4.31, 4.32 and 4.33 all show high number of F_n cases which shows why the recall for all three categories is small. Another interesting finding is that the algorithm predictions are highly precised which shows that when the algorithm is able to detect a given label its detection is precisely where the object is expected to be. Lastly, it is important to mention that in order for the onboard processing to work it was noted that the object needs to be within 1 meter or less of the quadcopter. This makes onboard image processing tricky as it is difficult to maneuver a quadcopter that close to an overhead power line tower. In addition, to this the safety of the quadcopter and also of the transmission line comes into question as well. Weather conditions will also now play an important role, since the proximity of the quadcopter and the tower is not that big it would be advisable not to fly the quadcopter in extremely windy conditions that may cause the quadcopter to loose control and in worst case scenario fly into the power tower itself.

4.7. Test 7: Insulator Inspection Via Quadcopter (Ground station)

This particular test was carried out using the Q2F-00013 camera. To test different scenarios with the quadcopter. Figure 4.35 shows the precision-recall curve for all three labels for test 7. Figure 4.36, 4.37 and 4.38 show the overall results for all three categories and Figure 4.39 shows 4 processed images from test 7 data set. In addition

to this Table 4.8 summarizes the results of test 7. As in the case of test 5 and 6, Test 7 and 8 were also carried out simultaneously.

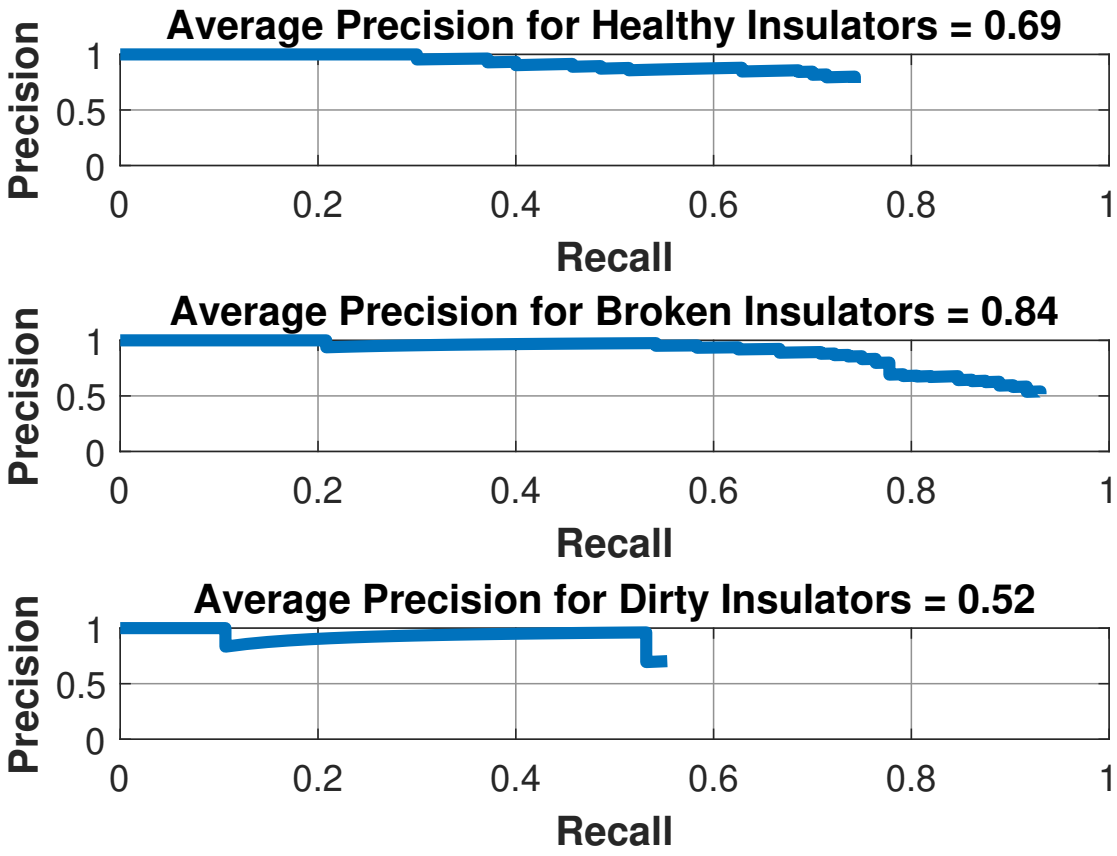

Figure 4.35: Precision-recall curve for all three categories for test 7.

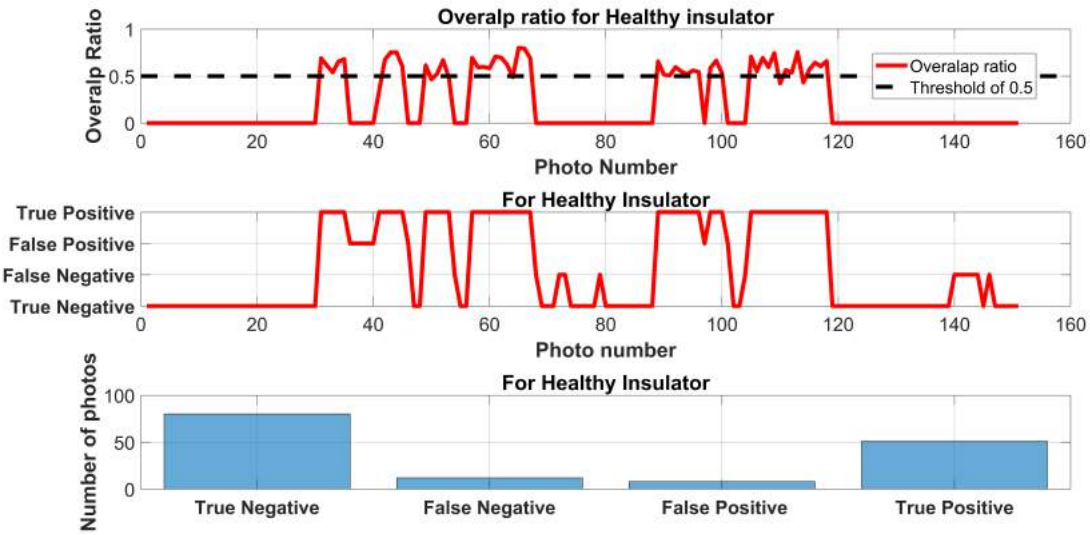

Figure 4.36: Test 7 overlap ratio and overall processing result for healthy insulators.

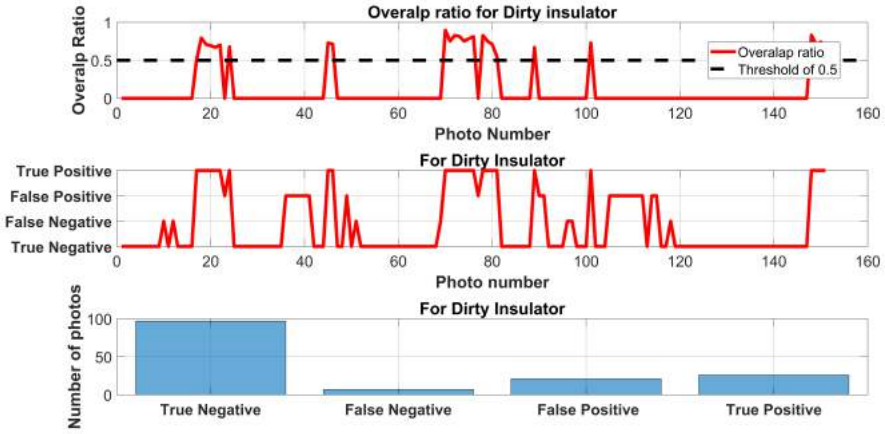

Figure 4.37: Test 7 overlap ratio and overall processing result for dirty insulators.

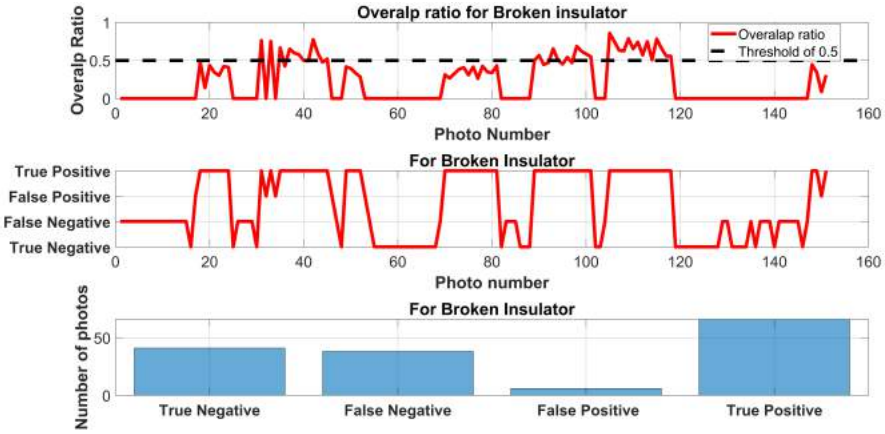

Figure 4.38: Test 7 overlap ratio and overall processing result for broken insulators.

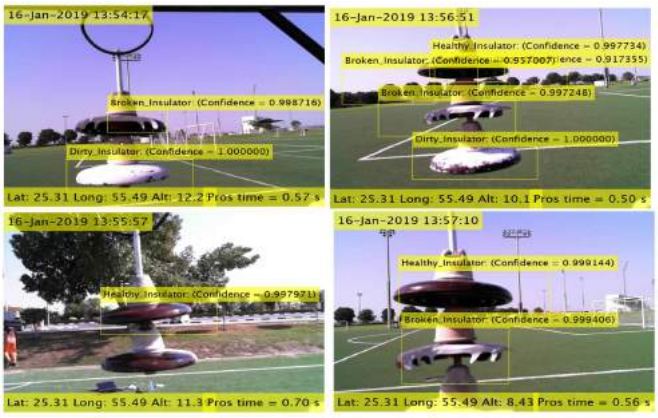

Figure 4.39: Four images from the overall 151 images that were processed from test 7.

Table 4.8: Data from insulator inspection test 7.

Attribute	Value
AP Healthy	0.69
AP Broken	0.89
AP Dirty	0.52
Average overlap ratio (Healthy)	0.60
Average overlap ratio (Broken)	0.50
Average overlap ratio (Dirty)	0.70
mAP	0.68
APT	0.53 seconds

4.8. Test 8: Insulator Inspection Via Quadcopter (Onboard)

This particular test was carried out using the Q2F-00013 camera. This test was carried out simultaneously with test 7 and the processing was done on the onboard Raspberry Pi. Discussion of this particular test is done in tandem with test 8.Figure 4.40 shows the precision-recall curve for all three labels for test 8. Figure 4.41, 4.42 and 4.43 show the overall results for all three categories and Figure 4.44 shows 4 processed images from test 8 data set. In addition to this Table 4.9 summarizes results in test 8.

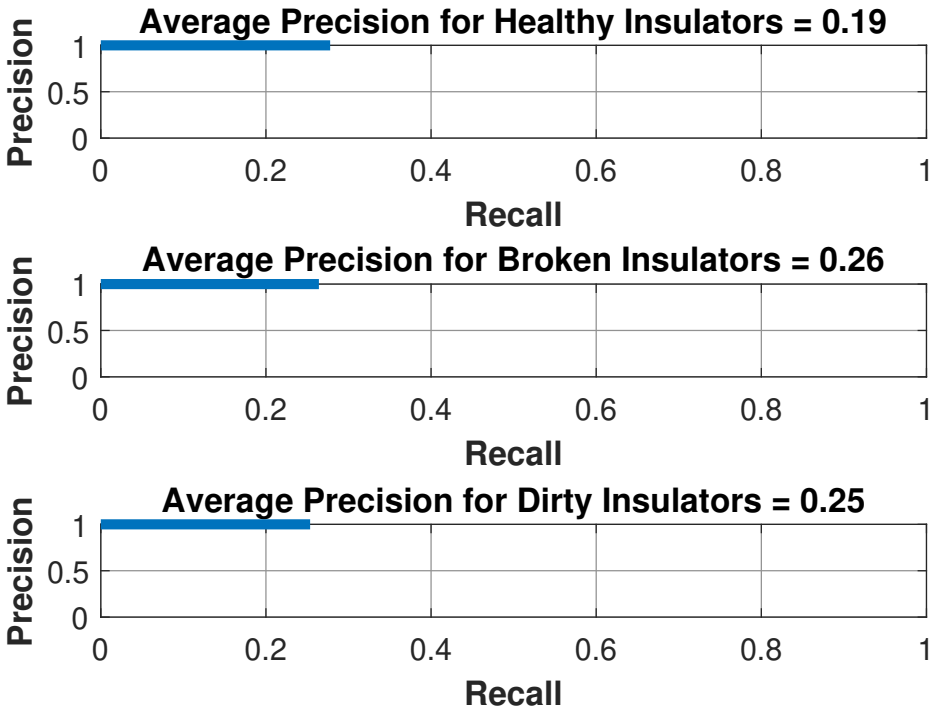

Figure 4.40: Precision-recall curve for all three categories for test 8.

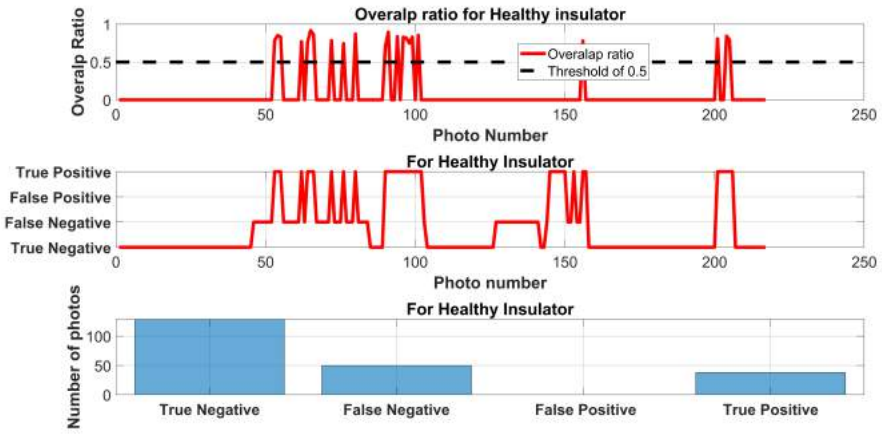

Figure 4.41: Test 8 overlap ratio and overall processing result for healthy insulators.

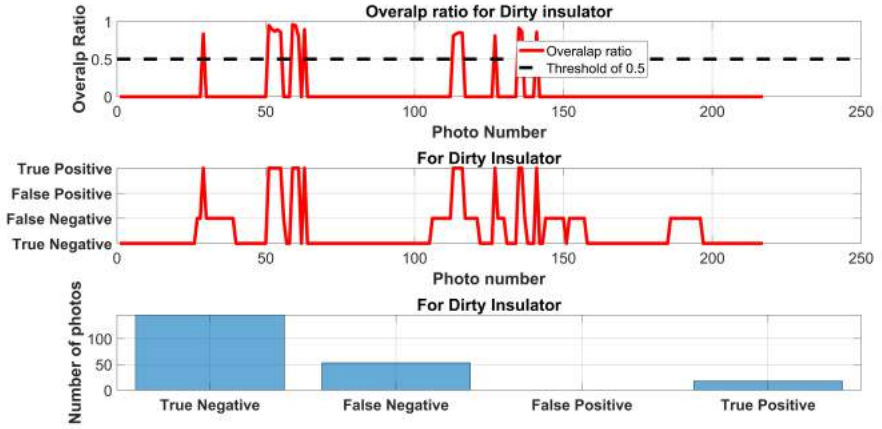

Figure 4.42: Test 8 overlap ratio and overall processing result for dirty insulators.

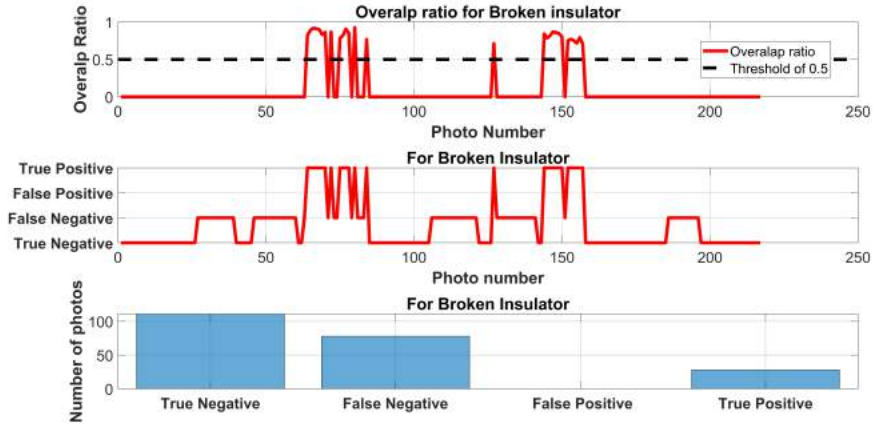

Figure 4.43: Test 8 overlap ratio and overall processing result for broken insulators.

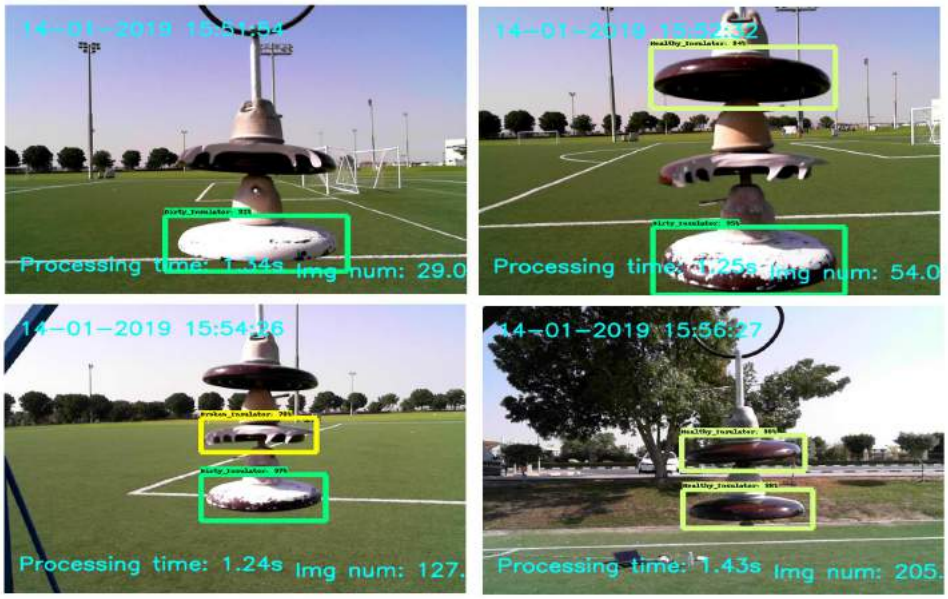

Figure 4.44: Four images from the overall 216 images that were processed from test 8.

Table 4.9: Data from insulator inspection test 8.

Attribute	**Value**
AP Healthy	0.19
AP Broken	0.26
AP Dirty	0.25
Average overlap ratio (Healthy)	0.78
Average overlap ratio (Broken)	0.80
Average overlap ratio (Dirty)	0.83
mAP	0.24
APT	1.28 seconds

Results from test 7 and 8 further tally with the findings from test 5 and 6. The image processing algorithm on Raspberry Pi has very high precision but its recall capability is very low as shown by results in Figures 4.41, 4.42 and 4.43. Another common factor found is that the processing time on Raspberry Pi is almost double the time it takes for the offshore processing. As expected due to the low recall capability in for all three categories in test 8 the mAP is quite low as shown in Table 4.9.

4.9. Score Threshold

As mentioned before various aspects need to be taken into account while processing an image. By default when an image processing algorithm detects an object in an image it attributes a score to its detection. The score values in Matlab lie between 0 to 1 which can be linked to percentage as well from 0 to 100%. If an algorithm is allowed to assign any score value between 0 and 1 then chances of F_p increase and so the precision of the overall label decreases. On the other hand, chances of F_n decreases meaning that recall capability of the system increases.

This causes a problem for the user. If an image processing algorithm is not very precise and the application which it is being used for requires high precision then the user can increase the precision of the system by setting a high score threshold. Doing so allows the user to overcome situations where an image data set contains a high number of F_p cases that may arise due to the lower score threshold value. In the same sense if an application requires high recall capability then the user can decrease the score threshold in order to decrease the number of F_n instances in an image data set. Consequently this leads to increase in the recall capability of the detection algorithm. It is however, important to keep in mind that variations in F_p instances can also be affected by changing the threshold on IoU results. By default an acceptable value is 0.5 as mentioned previously. However, a user can change it depending on application requirements.

Using ground truth image data set from test 3, ten different result data sets were formed where each data set had a unique score threshold from 0 to 0.9. This was done in order to find an ideal score threshold that should be implemented on the both offshore and onboard image processing algorithm. Figure 4.45 shows precision-recall curve for all three categorize for score threshold 0 to 0.5. Similarly, Figure 4.46 shows precision-recall curve for all three categorize for a score threshold of 0.6 to 0.9. From Figure 4.45 it can be observed that as score threshold increases the recall capability of the label decreases. This is true for all three labels. In the case of dirty insulator the difference is not that dominant but for healthy insulators the difference is clearly observed. The

change in recall is also prominent for broken insulators. With Figure 4.46 this change becomes more prominent in all three labels.

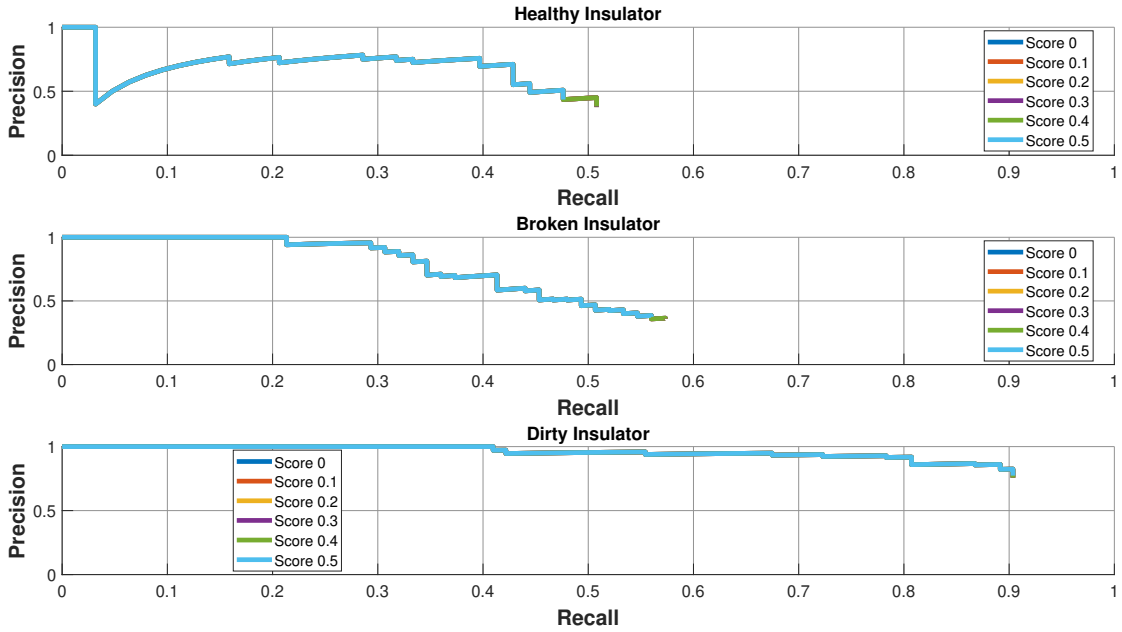

Figure 4.45: Graph showing precision-recall for score threshold values from 0 to 0.5.

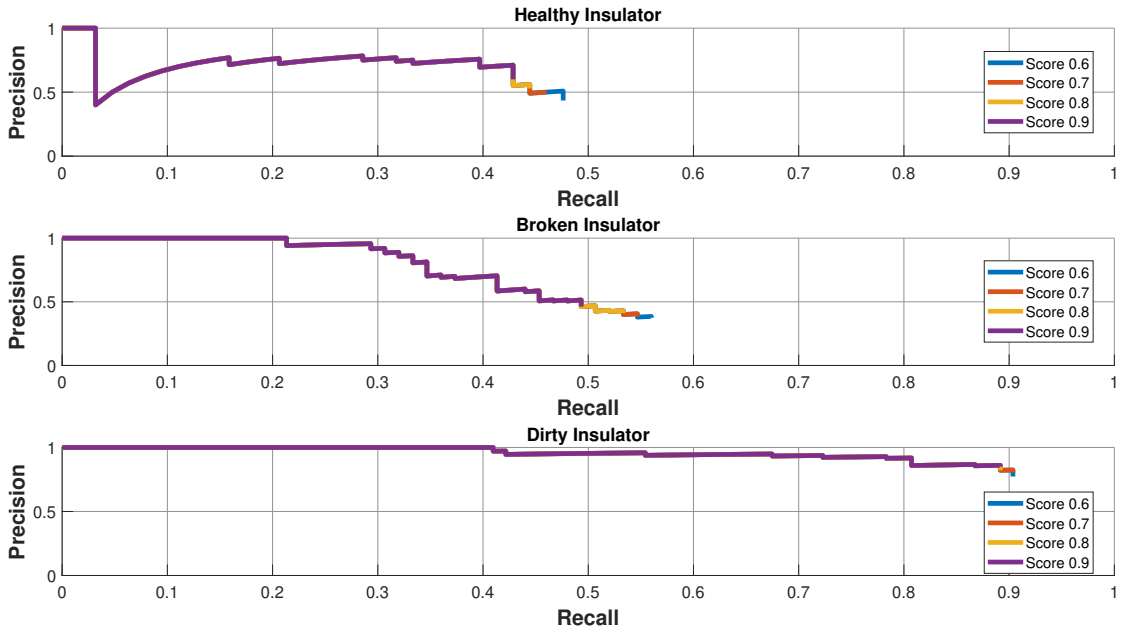

Figure 4.46: Graph showing precision-recall for score threshold values from 0.6 to 0.9.

Since our application requires the quadcopter to take multiple images of the same insulators present on overhead power lines, recall can be sacrificed for more precise results. Therefore using information from Figure 4.45 and 4.46 it was decided to use a score threshold of **0.85** in order to get more precises results and sacrifice recall.

4.10. Discussion on Results

All the results mentioned above are summarized in Table 4.10.

Table 4.10: Table summarizing results from tests 1-8.

Test no	mAP	Algorithm	Offshore/onboard	APT (seconds)
1	0.77	RCNN	Offshore	0.44
2	0.34	RCNN	Offshore	0.55
3	0.58	RCNN	Offshore	0.52
4	0.54	RCNN	Offshore	0.70
5	0.74	RCNN	Offshore	0.58
6	0.27	Mobilenet	Onboard	1.27
7	0.68	RCNN	Offshore	0.53
8	0.24	Mobilenet	Onboard	1.28

The results from all 8 test show that both algorithms are able to detect the health of overhead insulators. From test 2 it can be concluded that picture quality greatly affects the results of image processing algorithms. However, it should be noted that the algorithm was still able to perform as the results showed a fair amount of detection in all three categories. Test 1, 3, 4, 5 and 7 shows that offshore processing is more reliable and is fast, primarily because of the hardware, the image processing algorithm is working on. From the mAP values in Table 4.10 it can be concluded that offshore processing performs better if we exclude test no 2 the average mAP for Offshore processing is **0.66**. As per [65] AP value of 0.5 and above is considered good and therefore the value of 0.66 can be considered more than acceptable. The APT values of test 1, 2, 3, 4, 5 and 7 show that it takes around **0.55 seconds** for the ground station to processes an image. This value can be used to establish that for proper detection to occur, a user must keep the same position and orientation of the quadcopter for around 0.7 seconds. However, it

should be taken into account that a user should to take multiple images of the overhead power line insulators in order for the algorithm to have more precise data.

Results from Raspberry Pi show that onboard processing on quadcopter is possible however, the speed of the processing and the recall capability of the hardware is of concern. Results from Table 4.7 and 4.9 show the precision of the algorithm running on the Raspberry Pi is very high however, the recall capability of the system is very low. Due to the very low recall capability the mAP for test 6 and 8 is very low as shown in Table 4.10, when compared to the offshore processing. It is however, worth mentioning that the precision of the algorithm is very high for all three labels. The average mAP for the two onboard tests shown in Table 4.10 is **0.26**. This value however, is an improvement to the mAP given by [66] which states that the expected mAP for MobileNetV2 SSD is around 0.22. The APT values in Table 4.10 show that it takes around **1.28 seconds** for the onboard processing to processes an image. Therefore, the user needs to maintain the quadcopter position and orientation for around 1.5 seconds in order for the onboard processing to properly processes an image. However, as the recall capability of the onboard processing is not very high in certain cases the quadcopter may need to stay in the same position for longer periods. However, the exact time required cannot be provided as this requires further testing that focuses on this particular problem.

Chapter 5: Concluding Remarks and Future Work

5.1. Conclusion

This thesis successfully built a quadcopter based system that can detect the health of insulators on overhead power line towers. The results show that the image processing algorithms that have been developed are able to correctly identify the health of overhead power line insulators. Both image processing techniques developed in this thesis have successfully been implemented on the Gapter based quadcopter system and results show that actual health identification of insulators from flight images can be carried out. For offshore processing the average mAP noted is 0.66 and for onboard processing the average mAP is 0.26. The APT of an image for offshore processing is 0.55 seconds, whereas for onboard processing it is 1.28 seconds. In the case of offshore processing, the detection of healthy insulators is the worst among all three label categories. This however, can be rectified by further training the algorithm and introducing more variables into the training data set. With regards to onboard processing the precision of the algorithm is better when compared with offshore processing. However, the recall capability of the MobileNetV2 net is lower than offshore processing, and the onboard APT is also higher than the one observed for offshore processing. Overall the main objectives of this thesis have been achieved as shown by the results obtained.

5.2. Future Work

The major contribution made by this thesis is the overall development of a quadcopter based system that is able to detect the health of insulators on overhead power line towers. A considerable part of the work presented in this thesis lies in the development of the two particular image processing algorithms that are able to detect the health of an overhead power line insulator. The results produced in this work can be advanced by considering improved onboard hardware systems, using more advanced image detection and classification algorithms for improving the mAP. Also, autonomous flight of the quadcopter with guaranteed automatic maintenance of separation between the drone and the power line can be researched.

References

[1] M. Chavers, "Consumer Drones By the Numbers in 2018 and Beyond," Oct. 13, 2018. [Online]. Available: https://www.newsledge.com/consumer-drones-2018-numbers/. [Accessed: Jan. 31, 2019].

[2] S. Mukhopadhyay, S. Fernandes, M. Shihab, and D. Waleed, "Using Small Capacity Fuel Cells Onboard Drones for Battery Cooling: An Experimental Study," *Applied Sciences*, vol. 8, no. 6, p. 942, 2018.

[3] Z. Sarris and S. Atlas, "Survey of UAV applications in civil markets," in *The 9th IEEE Mediterranean Conference on Control and Automation*, Dubrovnik, Croatia, 2001, pp. 1–11.

[4] J. J. Xiong and E. H. Zheng, "Position and attitude tracking control for a quadrotor UAV," *ISA transactions*, vol. 53, no. 3, pp. 725–731, 2014.

[5] E. Semsch, M. Jakob, D. Pavlicek, and M. Pechoucek, "Autonomous UAV Surveillance in Complex Urban Environments," in *Proceedings of the 2009 IEEE/WIC/ACM International Joint Conference on Web Intelligence and Intelligent Agent Technology - Volume 02*, ser. WI-IAT '09. Washington, DC, USA: IEEE Computer Society, 2009, pp. 82–85. [Online]. Available: http://dx.doi.org/10.1109/WI-IAT.2009.132 [Accessed: 13-February-2019].

[6] S. Sabikan and S. Nawawi, "Open-Source Project (OSPs) Platform for Outdoor Quadcopter," *Journal of Advanced Research Design*, vol. 24, pp. 13–27, 2016.

[7] L. F. Luque-Vega, B. Castillo-Toledo, A. Loukianov, and L. E. Gonzalez-Jimenez, "Power line inspection via an unmanned aerial system based on the quadrotor helicopter," in *MELECON 2014-2014 17th IEEE Mediterranean Electrotechnical Conference*. Beirut, Lebanon: IEEE, 2014, pp. 393–397.

[8] L. Matikainen, M. Lehtomäki, E. Ahokas, J. Hyyppä, M. Karjalainen, A. Jaakkola, A. Kukko, and T. Heinonen, "Remote sensing methods for power line corridor surveys," *ISPRS Journal of Photogrammetry and Remote Sensing*, vol. 119, pp. 10–31, 2016.

[9] J. Katrasnik, F. Pernus, and B. Likar, "A Survey of Mobile Robots for Distribution Power Line Inspection," *IEEE Transactions on Power Delivery*, vol. 25, no. 1, pp. 485–493, 2010.

[10] C. Whitworth, A. Duller, D. Jones, and G. Earp, "Aerial Video Inspection of Overhead Power Lines," *Power Engineering Journal*, vol. 15, no. 1, pp. 25–32, 2001.

[11] R. Ishino and F. Tsutsumi, "Detection system of damaged cables using video obtained from an aerial inspection of transmission lines," in *Proceedings of the IEEE Power Engineering Society General Meeting*, Denver, CO, USA, 2004.

[12] D. Jones, "Power line inspection-a UAV concept," in *2005 The IEEE Forum on Autonomous Systems (Ref. No. 2005/11271)*. London, U.K: IET, 2005, pp. 1–8.

[13] I. Golightly and D. Jones, "Visual control of an unmanned aerial vehicle for power line inspection," in *ICAR'05. Proceedings., 12th International Conference on Advanced Robotics*. Seattle, WA, USA: IEEE, 2005, pp. 288–295.

[14] D. Jones, I. Golightly, J. Roberts, and K. Usher, "Modeling and control of a robotic power line inspection vehicle," in *2006 IEEE Conference on Computer Aided Control System Design, 2006 IEEE International Conference on Control Applications, 2006 IEEE International Symposium on Intelligent Control*. Munich, Germany: IEEE, 2006, pp. 632–637.

[15] M. Williams, D. Jones, and G. Earp, "Obstacle Avoidance During Aerial Inspection of Power Lines," *Aircraft Engineering and Aerospace Technology*, vol. 73, no. 5, pp. 472–479, 2001.

[16] M. J. B. Reddy, B. K. Chandra, and D. Mohanta, "A DOST Based Approach for The Condition Monitoring of 11 kV Distribution Line Insulators," *IEEE Transactions on Dielectrics and Electrical Insulation*, vol. 18, no. 2, pp. 588–595, 2011.

[17] V. S. Murthy, K. Tarakanath, D. Mohanta, and S. Gupta, "Insulator Condition Analysis for Overhead Distribution Lines Using Combined Wavelet Support Vector Machine (SVM)," *IEEE Transactions on Dielectrics and Electrical Insulation*, vol. 17, no. 1, pp. 89–99, 2010.

[18] Y. Yao, W. Wang, F. Chen, and Y. Yu, "Nondestructive testing of transmission lines based on the image method," in *2011 International Conference on Electronics, Communications and Control (ICECC)*, Ningbo, China, 2011, pp. 2143–2146.

[19] J. Mackevich and M. Shah, "Polymer Outdoor Insulating Materials. Part I: Comparison of Porcelain and Polymer Electrical Insulation," *IEEE Electrical Insulation Magazine*, vol. 13, no. 3, pp. 5–12, May 1997.

[20] I. Electronics, "Ultimate Guide to Electric Power Engineering: Transmission System: Insulators and Accessories," Industrial Electronics. [Online]. Available: http://www.industrial-electronics.com/elec_pwr_3e_11.html [Accessed: Apr. 9, 2019].

[21] M. Amin, M. Akbar, and M. N. Khan, "Aging Investigations of Polymeric Insulators: Overview and Bibliography," *IEEE Electrical Insulation Magazine*, vol. 23, no. 4, p. 44, 2007.

[22] Hebei Junai Power Technology Co.Ltd, "Polymer Pin Post Insulator." [Online]. Available: http://www.junai-china.com/channel.asp?id=53 [Accessed: Jan. 31, 2019].

[23] M. Rycroft, "Compact AC transmission lines provide solutions to servitude problems," EE Publishers. [Online]. Available: https://www.ee.co.za/article/compact-ac-transmission-lines-provide-solutions-to-servitude-problems.html [Accessed: Apr. 9, 2019].

[24] Electrical4U, "Types of Insulators Used in Overhead Lines," Electrical4U, Jan. 7, 2019. [Online]. Available: https://www.electrical4u.com/types-of-electrical-insulator-overhead-insulator/ [Accessed: Jan. 31, 2019].

[25] K. Daware, "Insulators used in overhead power lines," Electrical Easy. [Online]. Available: https://www.electricaleasy.com/2016/10/insulators-used-in-overhead-power-lines.html [Accessed: Apr. 9, 2019].

[26] S. Han, R. Hao, and J. Lee, "Inspection of Insulators on High-Voltage Power Transmission Lines," *IEEE Transactions on Power Delivery*, vol. 24, no. 4, pp. 2319–2327, 2009.

[27] R. Aggarwal, A. Johns, J. Jayasinghe, and W. Su, "An Overview of The Condition Monitoring of Overhead Lines," *Electric Power Systems Research*, vol. 53, no. 1, pp. 15–22, 2000.

[28] E. Cherney, A. Baker, B. Freimark, R. Gorur, Z. Lodi, M. Marzinotto, I. Ramirez-Vazquez, and G. Stewart, "Evaluation of and Replacement Strategies For Aged High-Voltage Toughened Glass-Suspension Insulators," *IEEE Transactions on Power Delivery*, vol. 30, no. 3, pp. 1145–1152, 2015.

[29] N. Mavrikakis, K. Siderakis, D. Pylarinos, and E. Koudoumas, "Assessment of field aged composite insulators condition in Crete," in *9th International Conference on Deregulated Electricity Market Issues in South Eastern Europe*, Nicosia, Cyprus, 2014, pp. 25–26.

[30] S. Gubanski, A. Dernfalk, J. Andersson, and H. Hillborg, "Diagnostic Methods for Outdoor Polymeric Insulators," *IEEE Transactions on Dielectrics and Electrical Insulation*, vol. 14, no. 5, pp. 1065–1080, 2007.

[31] INMR, "12 Examples of Insulator Failure," Jan. 7, 2019. [Online]. Available: http://www.ctcinsulator.com/ctcinsulator/en/newsshow.asp?id=31 [Accessed: Jan. 31, 2019].

[32] N. Hou, "The infrared thermography diagnostic technique of high-voltage electrical equipments with internal faults," in *POWERCON '98. 1998 International Conference on Power System Technology. Proceedings (Cat. No.98EX151)*, vol. 1, Bejing, China, 1998, pp. 110–115 vol.1.

[33] F. Schmuck, J. Seifert, I. Gutman, and A. Pigini, "Assessment of the condition of overhead line composite insulators," in *Cigre Session*, Paris, France, 2012, pp. 1–11.

[34] Matlab, "Compute bounding box overlap ratio using (bboxOverlapRatio)," MathWorks. [Online]. Available: https://www.mathworks.com/help/vision/ref/bboxoverlapratio.html [Accessed: Mar. 1, 2019].

[35] E. Alionte and C. Lazar, "A practical implementation of face detection by using Matlab cascade object detector," in *2015 19th International Conference on System Theory, Control and Computing (ICSTCC)*, Cheile Gradistei, Romania, 2015, pp. 785–790.

[36] Matlab, "Object Detection in a Cluttered Scene Using Point Feature Matching." [Online]. Available: https://www.mathworks.com/help/vision/examples/object-detection-in-a-cluttered-scene-using-point-feature-matching.html [Accessed: Mar. 3, 2019].

[37] A. Suneja and G. Kumar, " An Experimental Study of Edge Detection Methods in Digital Image," *Global Journal of Computer Science and Technology*, 2010. [Online]. Available: https://computerresearch.org/index.php/computer/article/view/894 [Accessed: 3-March-2019].

[38] X. Y. Xiao, R. Hu, S. W. Zhang, and X. F. Wang, "HOG-Based Approach for Leaf Classification," in *Advanced intelligent computing theories and applications. with aspects of artificial intelligence*. Springer, 2010, pp. 149–155.

[39] P. Dollar, R. Appel, S. Belongie, and P. Perona, "Fast Feature Pyramids for Object Detection," *IEEE Transactions on Pattern Analysis and Machine Intelligence*, vol. 36, no. 8, pp. 1532–1545, Aug 2014.

[40] Matlab, "Object Detection Using Deep Learning," Seo. 17, 2016. [Online]. Available: https://www.mathworks.com/help/vision/examples/object-detection-using-deep-learning.html [Accessed: Mar. 4, 2019].

[41] A. Krizhevsky and G. Hinton, "Learning multiple layers of features from tiny images," Citeseer, Tech. Rep., 2009.

[42] E. Electronics, "How to Set Up TensorFlow Object Detection on the Raspberry Pi," YouTube. [Online]. Available: https://www.youtube.com/watch?v=npZ-8Nj1YwY&feature=youtu.be [Accessed: Mar. 4, 2019].

[43] Pkulzc, R. Vivek, and W. Neal, "Tensorflow detection model zoo," GitHub. [Online]. Available: https://github.com/tensorflow/models/blob/master/research/object_detection/g3doc/detection_model_zoo.md [Accessed: Mar. 4, 2019].

[44] A. Gibiansky, "Quadcopter dynamics, simulation, and control," *Andrew. gibiansky. com*, 2012.

[45] T. Luukkonen, "Modelling and control of quadcopter," *Independent research project in applied mathematics, Espoo*, vol. 22, 2011.

[46] D. Gheorghi, I. Vntu, L. Mirea, and C. Brescu, "Quadcopter control system," in *2015 19th International Conference on System Theory, Control and Computing (ICSTCC)*, Cheile Gradistei, Romania, 2015, pp. 421–426.

[47] K. M. Thu and A. Gavrilov, "Designing and Modeling of Quadcopter Control System Using L1 Adaptive Control," *Procedia Computer Science*, vol. 103, pp. 528–535, 2017.

[48] Rcmoment, "High Performance DIY FPV 260 Mini Quadcopter Frame Kit 260mm." [Online]. Available: https://www.rcmoment.com/p-rm2071.html [Accessed: Feb.7, 2019].

[49] Y. Komatsuzaki, T. Doi, and K. Tadakuma, "Sensor based controlled leg type automatic landing system for aerial vehicles," in *2016 IEEE SENSORS*, Orlando, FL, USA, 2016, pp. 1–3.

[50] E. Kuantama, D. Craciun, I. Tarca, and R. Tarca, "Quadcopter Propeller Design and Performance Analysis," in *New Advances in Mechanisms, Mechanical Transmissions and Robotics*. Springer, 2017, pp. 269–277.

[51] Getfpv, "APC 16x5.5MR," Jan. 7, 2019. [Online]. Available: https://www.getfpv.com/apc-16x5-5mr.html [Accessed: Feb. 7, 2019].

[52] V. Kadamatt, "Best flight controller for quadcopter [2018] : How do I choose?" Dec. 13, 2018. [Online]. Available: http://www.droneybee.com/best-flight-controller-quadcopter/ [Accessed: Feb. 10, 2019].

[53] A. Jones, J. Van Valin, P. K. Komla, and A. Luther, "Modular drone and methods for use," U.S. Patent 9 533 759, January 3, 2017.

[54] D. Linden, *Handbook of Batteries*, 3rd ed., T. B.Reddy, Ed. McGraw-Hill, 2002.

[55] Gens, "TATTU 1800mAh 11.1V 45C 3S1P Lipo Battery Pack." [Online]. Available: https://www.gensace.de/tattu-1800mah-11-1v-45c-3s1p-lipo-battery-pack.html [Accessed: Feb. 10, 2019].

[56] P. Yedamale, "Brushless DC (BLDC) motor fundamentals," *Microchip Technology Inc*, vol. 20, pp. 3–15, 2003.

[57] Ebay, "E-flite BL15 Brushless Outrunner Motor 900Kv," Dec. 27, 2018. [Online]. Available: https://www.ebay.com/itm/E-flite-BL15-Brushless-Outrunner-Motor-900Kv-/253174655542 [Accessed: Feb. 11, 2019].

[58] H. Drone and Rover, "Drone kit contents," Nov. 9, 2018. [Online]. Available: https://nxp.gitbook.io/hovergames/userguide/getting-started/drone-kit-contents [Accessed: Feb. 13, 2019].

[59] B&H, "DJI GPS Module." [Online]. Available: https://www.bhphotovideo.com/c/product/1024806-REG/dji_part1_gps_module_for_phantom.html [Accessed: Feb. 13, 2019].

[60] Amazon, "Radiolink AT9S Transmitter." [Online]. Available: https://www.amazon.co.uk/Radiolink-Transmitter-Receiver-Quadcopter-LITEBEE/dp/B07196PZBP [Accessed: Feb. 13, 2019].

[61] Amazon, "YKS 3DR Radio Telemetry Kit 915Mhz Module." [Online]. Available: https://www.amazon.com/YKS-Telemetry-915Mhz-Pixhawk-Quadcopter/dp/B0196LF6PW [Accessed: Feb. 13, 2019].

[62] Gapter, "GAPTER: Gapter Brain and Internal Hardware Connection," Gaitech EDU. [Online]. Available: http://edu.gaitech.hk/gapter/internal-hardware-connections.html [Accessed: Mar. 5, 2019].

[63] Microsoft, “LifeCam Studio,” Microsoft, Apr. 19, 2011. [Online]. Available: https://www.microsoft.com/accessories/en-us/products/webcams/lifecam-studio/q2f-00013 [Accessed: Mar. 7, 2019].

[64] W. X. Vision, “Xinwei Vision WX071 Industrial-grade Macro HD camera USB Drive-free Android camera ID photo,” ChinaHao. [Online]. Available: https://www.chinahao.com/product/549527015964/ [Accessed: Mar. 7, 2019].

[65] M. Everingham, L. Van Gool, C. K. Williams, J. Winn, and A. Zisserman, “The pascal visual object classes (voc) challenge,” *International journal of computer vision*, vol. 88, no. 2, pp. 303–338, 2010.

[66] S. Mark and H. Andrew, “Google AI Blog,” Google. [Online]. Available: https://ai.googleblog.com/2018/04/mobilenetv2-next-generation-of-on.html [Accessed: Apr. 10, 2019].

Vita

Danial Waleed was born in Pakistan. He received his primary and secondary education in Dubai, United Arab Emirates. He received his B.Sc. degree in Electrical Engineering from American University of Sharjah (AUS) in 2016.

He joined the Mechatronics Engineering M.Sc. program in September 2016 in AUS. During his time in the M.Sc. program, he served as a graduate teaching assistant for two years and spent one year as graduate research assistant. During his M.Sc. studies he published three journal papers including one in IEEE Sensor journal and one conference paper. He was also part of the team that won UAE AI and Robotics for Good Award (National category) in 2017. His research interests include control systems, adaptive control, UAVs, image processing, and robotics.